Cross-reactive sarbecovirus antibodies induced by mosaic RBD-nanoparticles

Chengcheng Fan[1#], Jennifer R. Keeffe[1#], Kathryn E. Malecek[1], Alexander A. Cohen[1], Anthony P. West, Jr.[1], Viren A. Baharani[2,3], Annie V. Rorick[1,5], Han Gao[1], Priyanthi N.P. Gnanapragasam[1], Semi Rho[1], Jaasiel Alvarez[1], Luisa N. Segovia[1], Theodora Hatziioannou[2], Paul D. Bieniasz[2,4], Pamela J. Bjorkman[1,6*]

Affiliations

[1]Division of Biology and Biological Engineering, California Institute of Technology, Pasadena, CA 91125, USA

[2]Laboratory of Retrovirology, The Rockefeller University, New York, NY 10065, USA

[3]Laboratory of Molecular Immunology, The Rockefeller University, New York, NY 10065, USA

[4]Howard Hughes Medical Institute, The Rockefeller University, New York, NY 10065, USA

[5]Present address: Department of Biochemistry, University of Washington, Seattle, WA 98195, USA

[6]Lead contact
[#]Authors contributed equally
[*]Correspondence: bjorkman@caltech.edu

Abstract

Therapeutic monoclonal antibodies (mAbs) against SARS-CoV-2 become obsolete as spike substitutions reduce antibody binding. To induce antibodies against conserved receptor-binding domain (RBD) regions for protection against SARS-CoV-2 variants of concern and zoonotic sarbecoviruses, we developed mosaic-8b RBD-nanoparticles presenting eight sarbecovirus RBDs arranged randomly on a 60-mer nanoparticle. Mosaic-8b immunizations protected animals from challenges from viruses whose RBDs were matched or mismatched to those on nanoparticles. Here, we describe neutralizing mAbs from mosaic-8b–immunized rabbits, some on par with Pemgarda (the only currently FDA-approved therapeutic mAb). Deep mutational scanning, *in vitro* selection of spike resistance mutations, and cryo-EM structures of spike-antibody complexes demonstrated targeting of conserved epitopes. Rabbit mAbs included critical D-gene segment features in common with human anti-RBD mAbs, despite rabbit genomes lacking an equivalent human D-gene segment. Thus, mosaic RBD-nanoparticle immunization coupled with multiplexed screening represent an efficient way to generate and select therapeutic pan-sarbecovirus and pan-SARS-2 variant mAbs.

Introduction

Monoclonal antibodies (mAbs) that neutralize SARS-CoV-2 (SARS-2) have been used therapeutically to protect immunocompromised individuals and treat severe COVID-19[1,2]. mAbs licensed for use in humans target the receptor-binding domain (RBD) of the viral spike trimer, the primary target of neutralizing Abs[3-13]. With the emergence of SARS-2 variants of concern (VOCs), including the heavily mutated Omicron VOCs[14-19], previously approved therapeutic mAbs show greatly reduced or completely abrogated neutralization potencies, resulting in withdrawal from clinical use[1]. Currently, only one anti-SARS-2 mAb, Pemgarda, is authorized by the FDA for humans, having been issued Emergency Use Authorization (EUA) in March 2024[20]. Pemgarda and previous anti-spike mAbs were derived from Abs isolated from SARS-2 or SARS-CoV (SARS-1) infected human donors, in some cases after in vitro selection of variants that neutralize recent VOCs[1].

The degree of cross-reactive versus variant-specific properties of an anti-RBD Ab can be understood in the context of structural studies of coronavirus spike trimers and their interactions with Abs and the SARS-2 host receptor ACE2. After binding ACE2, spike induces fusion of the viral and host cell membranes after one or more of the spike RBDs adopt an "up" position that exposes the immunodominant receptor-binding motif (RBM) to allow interactions with ACE2. Many of the most potent neutralizing Abs recognize the RBM, thereby blocking ACE2 binding[4-8,11,12,21-25]. We used Fab-spike structures to define classes of neutralizing anti-RBD Abs (class 1, 2, 3, 4, and 1/4) based on their epitopes, overlap with the RBM, and recognition of up and/or down RBDs on spike trimers[22,26-28]. Notably, potent class 1 and class 2 anti-RBD Abs (e.g., previously licensed therapeutic mAbs[1]), recognize epitopes that overlap with the ACE2 binding footprint, a region that exhibits high sequence variability among sarbecoviruses and early SARS-2 VOCs[22]. By contrast, the epitopes of class 1/4, 4, the more recently-described class 5[29,30], and some class 3 Abs map to more conserved, but less accessible (in the case of class 1/4, 4, and 5 Abs), regions of sarbecovirus RBDs[22].

Targeting of conserved RBD regions could result in mAbs and vaccines that reduce the need for frequent updating. To preferentially elicit Abs against conserved epitopes, we developed mosaic-8b RBD nanoparticles (NPs) (Extended Data Fig. 1a), which display RBDs from eight different sarbecoviruses on 60-mer mi3 NPs, with the goal of stimulating B cell receptors that can crosslink using both antigen-binding Fabs between adjacent, non-identical, RBDs[31-33] (Extended Data Fig. 1b). We evaluated matched and mismatched immune responses (against viruses whose RBDs were or were not represented by an RBD on the NP), finding that mosaic-8b NPs showed enhanced heterologous binding, neutralization, and protection from sarbecovirus challenges compared with homotypic (SARS-2 RBD only) NPs in animal models[32,34]. Epitope mapping of polyclonal antisera elicited by mosaic-8b versus homotypic RBD-NPs using deep mutational scanning (DMS)[35] showed that mosaic-8b antisera primarily targeted more conserved class 4 and class 1/4 RBD epitopes that contact other portions of the spike trimer in down RBDs, whereas homotypic antiserum Abs mainly targeted variable, more accessible class 1 and 2 RBD epitopes that are not involved in intra-spike contacts[32].

Here, we describe immunization with mosaic-8b RBD-NPs as a process by which cross-reactive anti-sarbecovirus mAbs can be efficiently elicited as potential therapeutic reagents. We used single-cell optofluidics and multiplexed antigen specificity assays to profile antigen reactivity and assess the cross-reactivity of IgGs elicited by mosaic-8b in rabbits, finding a higher percentage of cross-reactive B cells for mosaic-8b compared with homotypic SARS-2 immunization (Fig. 1). We also mapped elicited mAb epitopes using competition ELISAs, DMS[35], 3D structure determinations, and *in vitro* selection[36,37] and evaluated neutralization against SARS-2 variants and other sarbecoviruses (Fig. 2-7), demonstrating that the mosaic RBD-NP vaccine approach works as designed to target conserved epitopes. Thus, when paired with a multiplexed antigen specificity assay to select for cross-reactivity, mosaic RBD-NP immunization could be used to efficiently develop therapeutic neutralizing mAbs that would not be affected by current or future SARS-2 VOC substitutions and would likely remain efficacious against a future sarbecovirus spillover.

Results

Mosaic-8b RBD-NPs elicit cross-reactive Abs

We covalently attached eight different sarbecovirus RBDs or only SARS-2 RBD to a SpyCatcher-mi3 NP[38,39] using the SpyCatcher-SpyTag system[38,39] to create mosaic or homotypic SARS-2 RBD-NPs[32,34] (Extended Data Fig. 1a). Mosaic-8b RBD-NPs included SARS-2 Beta RBD plus seven other sarbecovirus RBDs from clade 1a, 1b, or 2 spikes attached randomly to 60 positions on SpyCatcher-mi3[38], whereas homotypic SARS-2 RBD-NPs included only SARS-2 Beta RBD. In addition to previously-described characterization and validation[31,32,34], we used SpyCatcher- and mi3-specific mAbs and strain-specific RBD mAbs (Extended Data Fig. 1c,d, Extended Data Table 1) to confirm display of all 8 RBDs on mosaic-8b RBD-NPs and only SARS-2 Beta RBD on the SARS-2 RBD-NPs (Extended Data Fig 1e).

We next utilized a protocol to derive IgG heavy and light chain sequences from memory B cells of mosaic-8b–immunized rabbits in order to assess their potential for broad and potent anti-SARS-2 activity and to investigate whether the increased cross-reactivity of mAbs elicited by mosaic-8 observed in mice[33] extends to another species. Rabbits were primed and boosted with

mosaic-8b or SARS-2 RBD-NPs, and peripheral blood mononuclear cells (PBMCs) were isolated (Extended Data Fig. 1f). Memory B cells were enriched by IgG pulldown, and recovered cells were cultured to activate IgG secretion.

We used a Beacon optofluidics system to isolate and screen ~27,000 individual activated memory B cells for secretion of IgGs that recognized diverse sarbecovirus RBDs, both from unmatched strains (not represented by an RBD on mosaic-8b) and from matched strains (represented on the mosaic-8b or homotypic SARS-2 RBD-NPs) (Fig. 1; Extended Data Fig. 2). Assays for Ab secretion and antigen specificity were used to identify nanopens (chambers within an optofluidic chip) containing single cells secreting an IgG that bound to labeled antigens (Fig. 1a). Multiplexed assays using four fluorophores enabled screening for IgG secretion and binding to 12 antigens (Fig. 1b). Signal from fluorescence channels were overlaid to determine B cell breadth (Fig. 1c). Binding of each antigen was assessed by the presence of a fluorescent bloom above a nanopen using Beacon integrated software and manual verification (Fig. 1d).

Using results from the multiplexed assays, we found that immunization with mosaic-8b resulted in a higher percentage of B cells that recognized a range of both matched and mismatched RBDs compared with homotypic SARS-2 immunization, while SARS-2 immunization resulted in a higher percentage of B cells that recognized the matched SARS-2 Beta RBD (Fig. 1e). In addition, mosaic-8b immunization resulted in a higher percentage of B cells that recognized multiple RBDs (i.e., broadly cross-reactive mAbs) compared with homotypic SARS-2 immunization (Fig. 1f).

From the mosaic-8b RBD-NP immunized rabbit sample, we exported 90 B cells secreting IgGs that bound to any of the 12 assayed antigens, first exporting cells secreting IgGs that bound >6, followed by cells making IgGs that bound fewer antigens. The variable heavy and variable light chain genes from the first 48 exported cells were amplified and sequenced. We isolated paired heavy and light chain genes for 14 RBD-binding mAbs and subcloned them into expression vectors encoding human IgG C_H1-C_H2-C_H3 domains and human C_L domains (for IgGs) or human C_H1 and human C_L domains (for Fabs) (Extended Data Fig. 2).

Rabbit mAbs are broadly cross-reactive

RBD recognition by 14 rabbit mAbs elicited by mosaic-8b RBD-NPs was assessed via ELISA to a panel of RBDs that included sarbecovirus RBDs from clade 1a, 1b, 2, and 3 and SARS-2 variants (Fig. 2a). Three mAbs (M8a-B1, M8a-B9, and M8a-C9) bound to all sarbecovirus RBDs tested with EC_{50} values <0.1 µg/mL, and several others bound broadly to clade 1a, 1b, and 2 RBDs, consistent with identification of cross-reactive B cells by the single-cell multiplexed assays, which were mostly predictive of ELISA results (Extended Data Fig. 3).

We further characterized mAbs to identify epitopes using a competition ELISA. Fabs derived from characterized human mAbs that recognize class 1, 2, 3, 4, 1/4, or 5[22,27,29,30] RBD epitopes were adsorbed on an ELISA plate and then incubated with SARS-2 RBD. IgGs cloned from rabbit memory B cells, control IgGs of known epitope, or a human ACE2-Fc protein[27] were added and assessed for binding (Fig. 2b). In this assay, an IgG or ACE2-Fc will only bind if it is not sterically occluded by the bound Fab. We identified likely epitopes of 12 mAbs on SARS-2 RBD including one class 2, two class 4, six class 5, one class 1/3 (competes with both class 1 and

class 3 mAbs), and two class 1/4 anti-RBD mAbs (Fig. 2b). These results are consistent with previous findings that many class 3, 4, 1/4, and 5 anti-RBD Abs exhibit breadth of binding to sarbecovirus RBDs[22,23,27,29,30,32-34,40].

We next evaluated neutralization potencies (as assessed by inhibitory concentrations at 50%, IC_{50} values) and breadth of the rabbit mAbs against a panel of SARS-2 VOCs and other sarbecoviruses using a pseudovirus neutralization assay that correlates with authentic virus neutralization[41]. Neutralization results (Fig. 2c) for particular mAbs were generally consistent with binding data (Fig. 2a). While the potencies of some mAbs were modest, M8b-A10 (class 4) and M8b-C9 (class 1/4) exhibited both potency and breadth across the panel of tested viruses (Fig. 2c). Our neutralization panel did not include pseudoviruses for clade 2 sarbecoviruses with unknown host receptors. However, ELISA binding showed that both M8b-A10 and M8b-C9 bound to the RBDs of clade 2 spikes, whereas Pemgarda showed weak or no binding to clade 2 RBDs (Fig. 2a), suggesting that this licensed therapeutic mAb would not be effective against a clade 2 sarbecovirus spillover.

DMS reveals multiple RBD epitopes

To further evaluate residues within conserved and variable RBD epitopes (Fig. 3a) targeted by the rabbit mAbs, we used DMS to map residues that affect recognition by five mAbs (M8b-A10, M8b-B1, M8b-B8, M8b-C9, and M8b-C10) using yeast display libraries derived from SARS-2 Beta RBD[42]. DMS revealed class 4 anti-RBD Ab epitope escape profiles with sensitivities to substitutions at RBD residues 378 and 411 (M8b-A10) and 411, 413, and 427 (M8b-C9) (Fig. 3b), consistent with their broad binding and neutralization (Fig. 2a,c) and competition ELISA classifications (Fig. 2b). DMS analysis of M8b-B1 showed that most escapes were mediated by substitutions that encoded a potential N-linked glycosylation site (PNGS) to add an N-glycan at RBD residue 357 (R357N) or 394 (Y396T) within the class 5 epitope (Fig. 3b), consistent with competition ELISA results (Fig. 2b) and M8b-B1's broad binding and neutralization properties (Fig. 2a,c). DMS for M8b-B8 indicated a class 1 anti-RBD Ab profile centered on RBD residue 504 (Fig. 3b). Finally, M8b-C10 showed a class 3 profile centered on residues 441, 499, and 500, and Pemgarda showed a class 1/3 profile centered on residues 408, 500, 503, and 504, consistent with competition ELISA epitope class assignments (Fig. 2b).

3D structures rationalize mAb properties

To further explore recognition and neutralization mechanisms, we solved 3.2 Å-3.5 Å resolution single-particle cryo-electron microscopy (cryo-EM) structures of rabbit mAb Fabs complexed with a SARS-2 spike-6P trimer[43] and 2.4 Å-2.6 Å resolution X-ray structures of Fab-RBD complexes (Fig. 4,5; Extended Data Fig. 4, Extended Data Tables 2,3). As previously observed for structures of infection- and vaccine-induced human mAb Fabs bound to SARS-2 spike trimers[22,25,44,45], the rabbit mAb Fab cryo-EM structures showed different modes of RBD recognition: M8b-A10, M8b-B8, and M8b-C9 Fabs bound to RBDs only when they were in an "up" conformation (Fig. 4a-c), and M8b-C10 Fab recognized both "up" and "down" RBDs (Fig. 4d). Because only dissociated trimers were observed on cryo-EM grids of M8b-B1 Fab incubated with a spike trimer, we determined a crystal structure of a M8b-B1 Fab-RBD complex (Fig. 4e).

The M8b-A10–spike cryo-EM structure revealed that each of the three "up" RBDs was recognized by an M8b-A10 Fab using all six of its complementarity-determining regions (heavy

chain CDRH1, CDRH2, and CDRH3 and light chain CDRL1, CDRL2, and CDRL3) and heavy chain framework region 1 (FWRH1) (Fig. 4a,g, Extended Data Fig. 5a). Consistent with competition ELISA and DMS results (Fig. 2b, 3b), the footprint of M8b-A10 on the RBD surface resembled that of a cross-reactive class 4 anti-RBD mAb, CR3022[40] (Fig. 4f,g), which was originally isolated from a SARS-1–infected patient[46]. Also consistent with M8b-A10's cross-reactive binding and neutralization properties (Fig. 2a,c), its binding footprint involved residues that are largely conserved across sarbecovirus RBDs (Fig. 3a,4g).

The M8b-B8 Fab-spike structure showed two Fabs binding to "up" RBDs with the third, non-Fab-bound, RBD adopting the "down" position (Fig. 4b). RBD recognition was mediated by both the V_H and V_L domains using all six CDRs plus FWRH1 (Fig. 4h, Extended Data Fig. 5b). We classified M8b-RBD as a class 1 anti-RBD Ab because the majority of RBD residues at the M8b-B8 epitope were residues from the variable class 1 epitope (RBD residues 403, 405, 415-417, 453, 455, 456, 489, 493, 498, 500-503, and 505), although two RBD residues (Y453 and Y489) overlapped with the variable class 2 RBD epitope and one residue (R408) overlapped with the more conserved class 4 RBD epitope (Fig. 3a, 4f,h, Extended Data Fig. 6a-c). This is consistent with competition ELISA results showing that M8b-B8 competed with mAbs from class 1, class 2, class 4, and class 1/4 mAbs (Fig. 2b). In addition, although their binding epitopes do not overlap, M8b-B8 competed with C110, a human class 3 anti-RBD mAb[22], likely due to steric clashes between the C_H1 and C_L domains of the bound Fabs (Extended Data Fig. 6d). Binding to non-conserved regions of the RBD contributed to limited binding of M8b-B8 to sarbecovirus RBDs by ELISA and weak neutralization potencies against a subset of sarbecoviruses and variants of SARS-2 (Fig. 2a,c).

We observed three M8b-C9 Fabs bound to spike in the cryo-EM structure, all recognizing "up" RBDs (Fig. 4c), as found for M8b-A10, which also recognized only "up" RBDs (Fig. 4a). To resolve high-resolution details of the Fab-RBD interaction, we solved a 2.6 Å crystal structure of an M8b-C9–SARS-2 RBD complex (Extended Data Table 3). Recognition of M8b-C9's class 1/4 RBD epitope was mediated mainly by its V_H domain (Fig. 4i) through heavy chain CDRH1, CDRH3, FWRH1, and FWRH2 and light chain CDRL2 and FWRL2 regions (Extended Data Fig. 5c). The identification of a class 1/4 epitope in the Fab-spike and Fab-RBD structures is consistent with competition for RBD binding with class 1 and class 4 anti-RBD mAbs (Fig. 2b), cross-reactive binding of M8b-C9 IgG to all spike proteins and RBDs (Fig. 2a), and broad neutralization of SARS-2 variants and other sarbecoviruses (Fig. 2c).

The M8b-C10 Fab-spike structure revealed Fabs binding to all spike RBDs, with two RBDs adopting an "up" conformation and the third RBD in the "down" conformation (Fig. 4d). The interaction between M8b-C10 and the RBD was mediated by its heavy chain CDRH1, CDRH2, CDRH3, and FWRH1 and light chain CDRL1 and CDRL2 (Fig. 4j, Extended Data Fig. 5d). As seen by comparing the outlines of Ab epitopes on an RBD surface (Fig. 4f), the M8b-C10 binding epitope overlaps with the epitopes of class 1 and class 3 anti-RBD mAbs, but not with epitopes of class 2 or class 4 mAbs (Extended Data Fig. 6e). This class 1/3 epitope (Fig. 2b) mostly involves residues that vary between sarbecoviruses (Fig. 3a), consistent with the limited RBD recognition observed by ELISA for M8b-C10 (Fig. 2a). Although the binding footprints of M8b-C10 and the class 2 mAb C002 do not overlap (Extended Data Fig. 6e), M8b-C10

competed with two class 2 mAbs for RBD binding (Fig. 2b), most likely due to steric clashes between Fab C_H1 and C_L domains.

The M8b-B1 Fab-RBD crystal structure showed recognition of an epitope on a side of RBD that is buried in "down" RBDs (Fig. 4e). The interaction between M8b-B1 and RBD was mediated by FWRH1 and all CDR loops except CDRL2 (Fig. 4k, Extended Data Fig. 5e). Modeling suggested that M8b-B1 Fab would clash with a neighboring NTD when recognizing a trimer with "up" RBDs (Extended Data Fig. 5f), consistent with M8b-B1 Fab incubation with spike resulting in dissociated spike trimers on cryo-EM grids. The structurally-identified M8b-B1 epitope (Fig. 4k) is consistent with competition with CC25.4 (Fig. 2b), which recognizes the partially conserved class 5 RBD epitope[29,30], and M8b-B1 cross-reactive binding and potent neutralization against most SARS-2 variants and other sarbecoviruses (Fig. 2a,c).

We also compared structures of the rabbit mAbs to structures of mAbs that were isolated from COVID-19 convalescent donors and FDA-approved mAbs (Fig. 5). M8b-A10 and M8b-C9 targeted similar regions of the RBDs as C118[27] and S2X259[47], two cross-reactive and potent mAbs that were isolated from convalescent human donors (Fig. 5a,b). Importantly, M8b-B8 and M8b-C10 both recognize epitopes similar to that of Pemgarda, the only currently FDA-approved therapeutic mAb for SARS-2 treatment[20], and Bebtelovimab, a previously FDA-approved anti-SARS-2 mAb[1] (Fig. 5a,b). M8b-B8 and Pemgarda share common epitope residues, including RBD residues 403, 405, 406, 408, 409, 415, 498, 500-505, and 508, and M8b-C10 and Pemgarda share RBD epitope residues 403, 439, 496, and 498-506. Although reside Q493 was not classified by PDBePISA[48] as part of the binding epitope of Pemgarda (Fig. 5c), a Q493E substitution was shown to contribute to Ab evasion of Pemgarda[49]. Only one of the rabbit mAbs (M8b-B8) targets an RBD epitope containing residue Q493 (Fig. 5d, Extended Data Fig. 5b).

Cross-species class 1/4 mAb features

Identification of rabbit (and previously mouse[33]) anti-RBD mAbs raised by mosaic-8 immunization offers the opportunity to compare their properties with those of human mAbs raised by SARS-2 infection and or COVID-19 vaccination; e.g., since V, D, and J gene segments can differ between species[50], it is of interest to ask whether recognition features are conserved in anti-RBD mAbs raised in different species.

Of relevance to this question, a public class of anti-SARS-2 human mAbs with a CDRH3 YYDxxG motif derived from the D gene segment of IGHD3-22 was identified[51,52] (Fig. 6). Human mAbs in this recurrent class, e.g., COVA1-16[26], C022[27], and ADI-622113[53] use the YYDxxG motif to recognize the class 1/4 RBD epitope by extending an RBD β-sheet through mainchain hydrogen bonding with a two-stranded antiparallel β-sheet formed by the CDRH3 (Fig. 6a-c), as originally described for a COVA1-16–RBD structure[26]. Structural comparisons of the interfaces of RBD with M8b-C9 (Fig. 6f) and ADI-62113[54] (Fig. 6c) revealed that heavy chain residues $Y98_{VH}$ and $Y99_{VH}$ in M8b-C9 interact with RBD with the same interface geometry as the tyrosines in the YYDxxG motif. A structural motif search for Abs with a YY motif in CDRH3 that interacts with RBD residues 378-382 found other examples: human mAbs CC25.36[54] (Fig. 6d) and S2X259[47] (Fig. 6e), as well as several nanobodies[55]. CC25.36 was also previously noted to use a CDRH3 YYDML motif to recognize RBD in a manner similar to YYDxxG Abs[54]. The genetic origins of the core YY features within CDRH3s vary: IGHD3-22

for YYDxxG motif Abs, IGHD3-9 for YYDML motif Abs, and a CDRH3 random library for the synthetic nanobodies. IMGT/V-Quest analysis[56] of the M8b-C9 V_H gene segment revealed that its YY motif derived from N region addition rather than from a D gene segment. The smallest core motif for the above Abs could be considered to be the tyrosine ($Y98_{VH}$ in M8b-C9) that interacts with the aliphatic portion of the RBD K378 sidechain in combination with adjacent backbone hydrogen bonds to RBD residues 378-379 that extend an antiparallel β-sheet of the RBD. This feature was described for mAb C118[27], which contains a YT CDRH3 sequence (Fig. 6g), and the structural motif search found additional cases: Ab AB-3467[28] (YS) (Fig. 6h) and Ab N3-1[57] (YF) (Fig. 6i). These comparisons provide examples in which the immune system converges upon similar recognition motifs derived either from different Ab gene segments or from processes such as N-region addition that occur during V-D-J recombination.

Selection reveals functional escapes

To investigate the sensitivity of the rabbit mAbs to viral escape, we conducted cell culture selection experiments[58,59] using a replication-competent recombinant vesicular stomatitis virus (rVSV) encoding the spike protein of either SARS-2 Wuhan-Hu-1, SARS-2 BA.2, SARS-2 XBB.1.5, or SARS-1[41]. For each experiment, the corresponding rVSV was allowed to replicate in the presence of a rabbit Ab at a concentration of its 10x IC_{50} value (Fig. 2c) to select for escape variants (Fig. 7). Consistent with structural results (Fig. 4a,g), M8b-A10 selected for escape at residues within the class 4 RBD epitope of both SARS-2 and SARS-1 spike-bearing viruses (Fig. 7a). Escape from M8b-A10 included substitutions at K378 (92.7% K378Q and 6.6% K378E in the Wuhan-Hu-1 chimeric virus), an RBD position that was identified as a key residue of escape using DMS (Fig. 3b), and at G413 (26.6% and 29.2% G413R in the BA.2 and XBB.1.5 contexts, respectively) and the equivalent residue in SARS-1, G400R (94.9% substitution). Selection in the presence of the class 5 mAb M8b-B1 resulted in viruses containing substitutions in the RBD outside of the mAb epitope, including P384L (46.6% substitution in Wuhan-Hu-1), as well as within the epitope (E465K, 59.3% substitution in XBB.1.5 and E452G or E452D, 97.9% substitution in SARS-1 viruses) (Fig. 7b). In contrast, DMS showed selection by addition of PNGSs within the epitope, substitutions that have not been seen to date in viral isolates[60], perhaps because N-glycan addition in the context of a replicating virus in viral isolates and in this selection system[58,59] could reduce viral fitness or infectivity. Escape from M8b-C9, a class 1/4 mAb, led to the acquisition of a G413R substitution in SARS-2 spikes (98.7% in Wuhan-Hu-1, 30.7% in BA.2, 98.6% in XBB.1.5) and D414V in SARS-1 (78.0%) (Fig. 7c). These RBD residues constitute some of the more variable positions within the conserved class 4 RBD epitope (Fig. 3a). Selection of SARS-2 chimeric viruses in the presence of M8b-C10, a class 1/3 mAb whose RBD binding footprint overlaps with that of Pemgarda (Fig. 5c), resulted in a virus with a P499Q substitution in Wuhan-Hu-1 RBD (100%) (Fig. 7d), which was also identified as a site of escape using DMS (Fig. 4b). Escape pathways of the BA.2-bearing virus were more diverse, with substitutions observed at 8 positions in and around the epitope, including residues in class 1, 3, and 4 RBD epitopes. Three substitutions observed during BA.2 selection in the presence of M8b-C10 were reversions to the Wuhan-Hu-1 sequence (A376T, N405D, S408R), and two additional substitutions are found in variant lineages (e.g., G446S in BA.1, XBB.1.5, KP.3; G496S in BA.1). With the exception of BA.2 selection in the presence of M8b-C10, all other substitutions observed in these selection experiments are seen only at low frequencies in natural sequences (<0.03%)[60].

Discussion

Therapeutic mAbs against the SARS-2 spike were beneficial for many during the COVID-19 pandemic[1,61]. However, emergence of previous, and likely future, VOCs with mutations that reduce mAb neutralizing activities against variants, along with recommendations against the use of single mAbs therapeutically[62], provide a compelling rationale to develop processes by which additional mAbs can be efficiently generated and identified, especially mAbs that broadly recognize RBDs from SARS-2 VOCs and animal sarbecoviruses.

As of 2024, the only approved mAb for COVID-19 treatment is Pemgarda, which is authorized for pre-exposure prophylaxis as a treatment option for immunocompromised individuals who do not make strong responses to vaccines[20]. However, given that Pemgarda's RBD epitope spans a region that exhibits variability (Fig. 3a, 5b), emergence of future VOCs are likely to limit its efficacy, consistent with a report that Pemgarda exhibits diminished neutralization of KP.3.1.1, a rapidly expanding VOC lineage[49]. Most therapeutic anti-SARS-2 mAbs have been isolated from infected and/or immunized human donors[63], in whom immune responses generally focus on the immunodominant, but variable, class 1 and class 2 RBD regions[4-8,11,12,21-25], thus usually resulting in mAbs that are sensitive to VOC substitutions. In addition, therapeutic mAbs developed against SARS-2 often required long development times; e.g., Pemgarda was engineered from a mAb originally isolated from a SARS-1 patient and then affinity matured[63,64], necessitating a multi-year process.

Here, we suggest a more directed and efficient approach to identifying cross-reactive mAbs; namely, immunizing with mosaic-8 NPs, which we have demonstrated direct Ab responses to more conserved RBD regions[31,32,34,65], and prescreening for breadth using a multiplexed binding assay. We previously reported identification of cross-reactive mAbs elicited in mice immunized with mosaic-8 NPs[33]. Here, we report discovery of promising mAbs exhibiting broad neutralization across animal sarbecoviruses derived from mosaic-8b–immunized rabbits. We chose rabbits for immunization because they have diverse Ab repertoires and were previously used for isolation of potent anti-SARS-2 spike RBD mAbs[66,67]. In the current study, we used multiplexed assays to evaluate binding to multiple antigens by IgGs secreted by individual B cells for comparing the breadth of responses to mosaic-8b versus homotypic SARS-2 RBD-NPs, finding broader responses for B cells from mosaic-8b– than homotypic SARS-2–immunized animals. In a screen of only 14 mAbs, we identified M8b-B8 and M8b-C10 with epitopes that overlap with and/or resemble Pemgarda's (Fig. 5a-c), as well as cross-reactive class 4 (M8b-A10) and class 1/4 (M8b-C9) mAbs (Fig. 2, 5a). A larger screen could be used to identify more mAbs with broadly cross-reactive neutralization profiles, which could be used therapeutically in combination. For identifying mosaic-8b–induced mAbs for therapeutic use in humans, mosaic-8b immunization could be done in transgenic human immune repertoire mice[68], wildtype animal-elicited mAbs could be humanized[69], and/or human mAbs isolated from participants in an upcoming mosaic-8b clinical trial funded by the Coalition for Epidemic Preparedness Initiative (CEPI).

Our results showed that differing Ab gene segment repertoires between humans and animals did not prevent mosaic-8b elicitation in rabbits of broadly cross-reactive Abs, including those with recognition properties similar to human anti-RBD Abs. For example, there is no apparent rabbit counterpart of the human D gene segment IGHD3-22, which encodes a common CDRH3

YYDxxG motif[52] that recognizes a class 1/4 RBD epitope by extending an RBD β-sheet through hydrogen bonding with an Ab CDRH3 β-strand. Yet with a relatively small screen, we found a rabbit mAb, M8b-C9, that uses a portion of the YYDxxG motif to extend the same RBD β-sheet using its CDRH3. In addition, two human mAbs, C022 and C118, exhibit RBD recognition properties resembling those of COVA1-16, yet only C022 contains the YYDxxG motif in its CDRH3[27]. Thus, the immune systems of humans and other mammals can utilize different Ab gene segments to arrive at similar modes of antigen recognition, underscoring the flexibility of mammalian Ab repertoires and suggesting that animal models can be used for screens to identify cross-reactive anti-RBD mAbs of potential therapeutic utility. It should also be possible to use a multiplexed assay, as described here, to select for broadly cross-reactive Abs from mosaic-8b–immunized humans as potential therapeutic mAbs.

Figures and legends

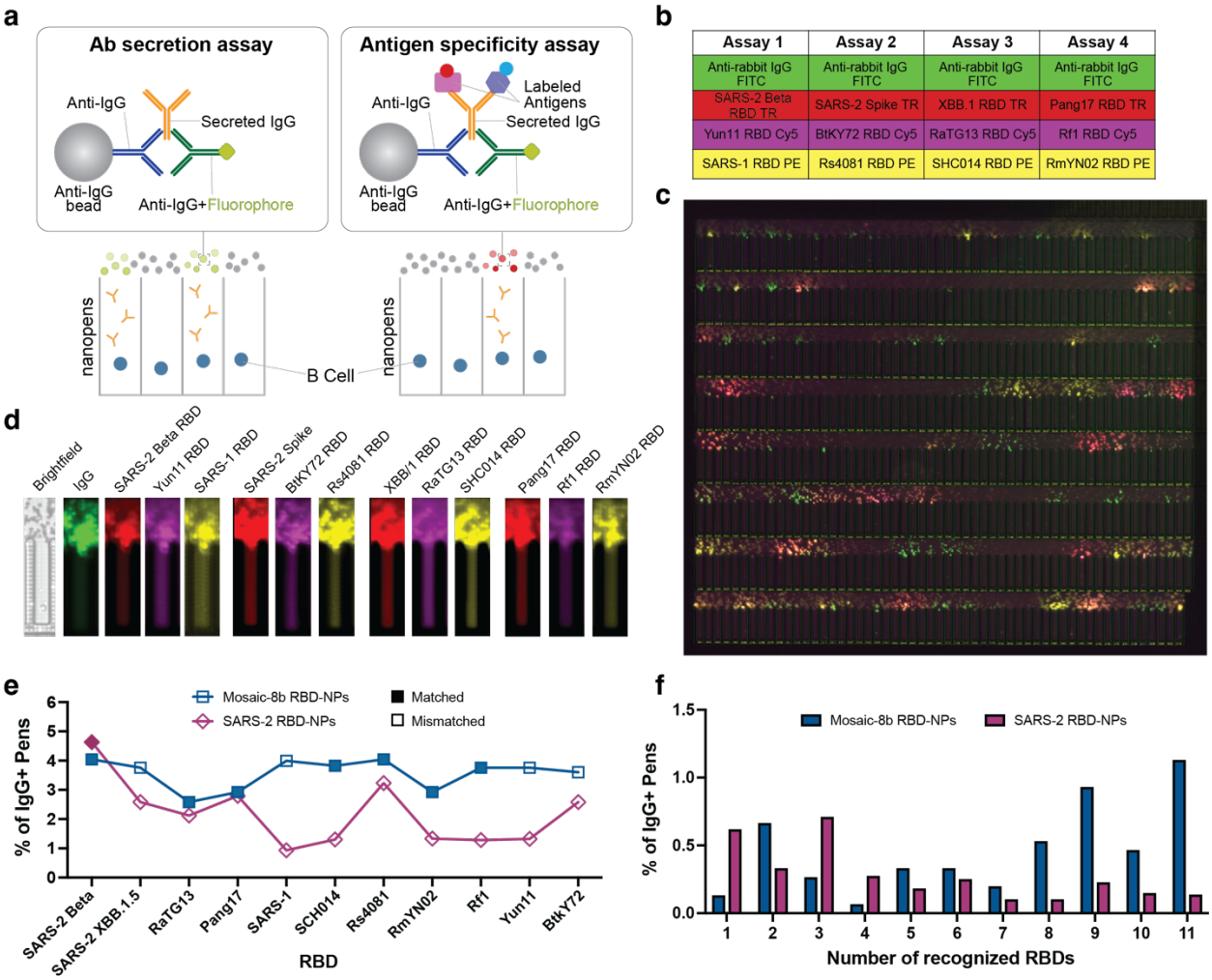

Figure 1. Rabbit memory B cells were characterized for secretion of broadly cross-reactive IgGs. Abbreviations. FITC: Fluorescein Isothiocyanate; TR: Texas Red; Cy5: Cyanine5; PE: Phycoerythrin. (a) Multiplexed assay to assess IgG binding breadth. Abs secreted from individual B cells in nanopens were captured by anti-rabbit IgG beads and detected with an anti-rabbit IgG secondary Ab conjugated to FITC or with antigens labeled with different fluorophores. (b) Four sequential assays for B cell screening, each of which assessed IgG secretion (FITC) and binding to three different antigens (labeled with TR, Cy5, or PE). (c) A field of view image from a multiplexed binding assay showing "blooms" above nanopens containing B cells secreting IgGs with different binding properties. (d) Individual nanopens were evaluated for antigen binding based on the presence of a bloom in fluorescent channels above the nanopen in sequential assays. Nanopens scored as positive for broad antigen binding were exported for cloning. (e) The percentage of IgG+ nanopens containing a single B cell that bind to each RBD in single-cell multiplexed assays comparing B cells from rabbits immunized with mosaic-8b RBD-NP (blue) or SARS-2 RBD-NP (mulberry). (f) The percentage of IgG+ nanopens that contain secreted IgG that recognize 1 to 11 RBDs from rabbits immunized with mosaic-8b RBD-NP (blue) or SARS-2 RBD-NP (mulberry).

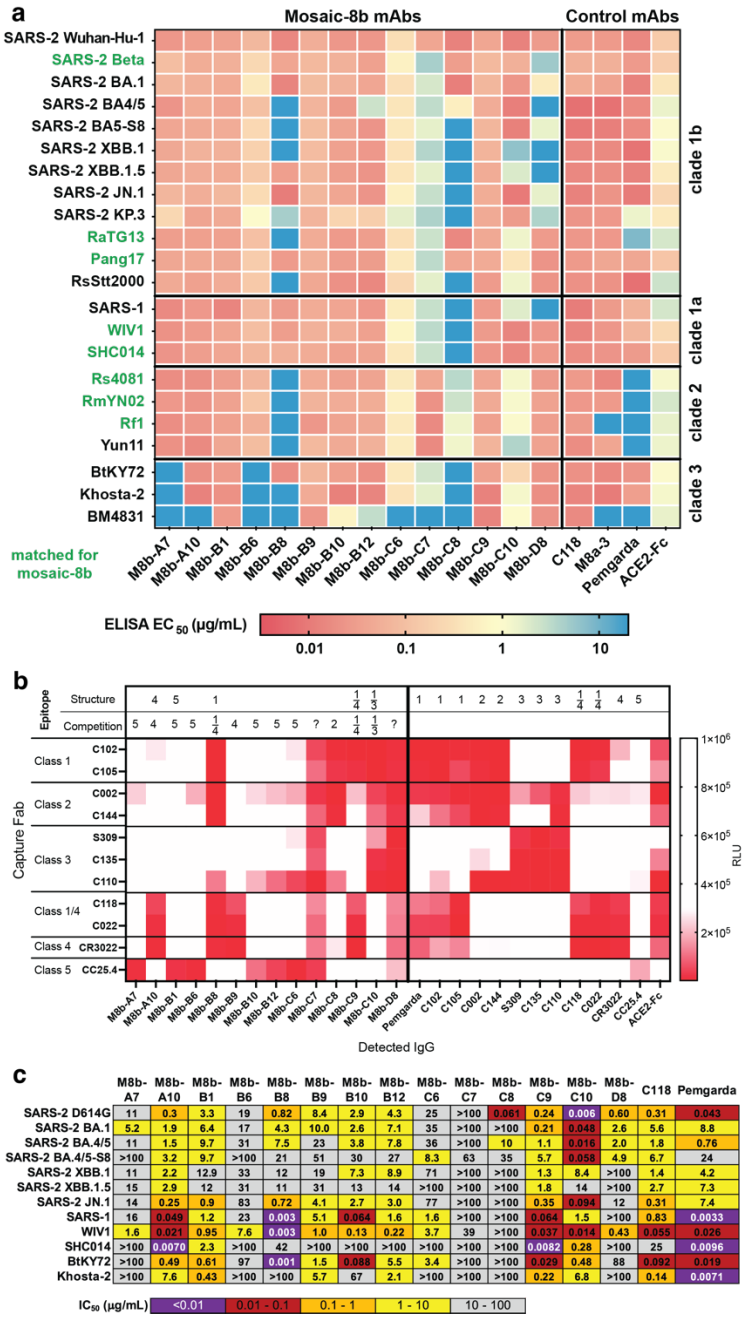

Figure 2. mAbs isolated from rabbits immunized with mosaic-8b exhibit broad recognition against SARS-2 and other sarbecoviruses.

(a) ELISAs to assess breadth of RBD binding of mAbs isolated from rabbits immunized with mosaic-8b RBD-NPs. (b) Competition ELISAs used to identify mAb epitopes. Immobilized Fab was used to capture SARS-2 RBD, IgGs indicated at the bottom were added, and Fc was detected. White: high luminescence signal indicating IgG binding does not compete with the Fab. Red: low signal indicating reduced binding consistent with competition. The RBD epitope class for each mAb is shown based on structural analysis (Structure) or competition ELISA (Competition). (c) Neutralization of rabbit mAbs against a panel of 12 pseudoviruses including SARS-2 D614G, five SARS-2 VOCs, three non-SARS-2 sarbecoviruses, and two pseudoviruses with chimeric spikes (BtKY72 or Khosta-2 RBD plus remainder of the SARS-1 spike).

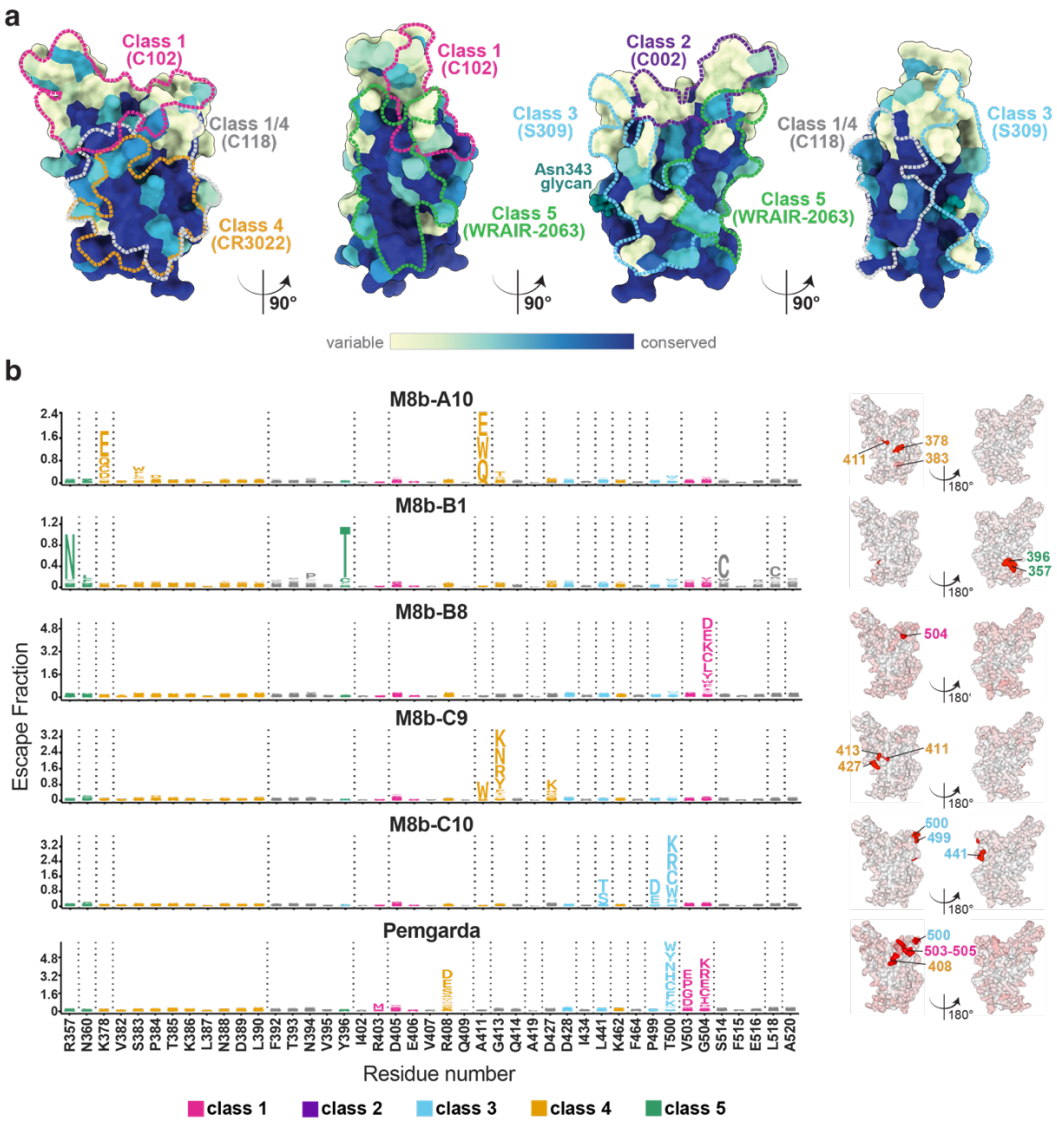

Figure 3. DMS of rabbit mAbs reveals RBD epitopes.
(a) Sequence conservation of 16 sarbecovirus RBDs calculated using ConSurf[70] and plotted on a surface representation of SARS-2 RBD (PDB 7BZ5). Epitopes for anti-RBD class 1, 2, 3, 4, 1/4, and 5 Ab epitopes[22,27,29,30] are outlined in dots in different colors using information from representative structures of mAbs bound to SARS-2 spike or RBD (C102: PDB 7K8M; C002: PDB 7K8T, S309: PDB 7JX3; CR3022: PDB 7LOP; C118: PDB 7RKV; WRAIR-2063: PDB 8EOO). (b) Results for experiments involving SARS-2 Beta yeast libraries. Left: Logo plot with RBD residue number (x-axis) and a stack of letters at RBD positions indicating amino acid substitutions that result in escape. The height of each letter indicates the degree of contribution for escape resulting from a particular substitution. The height of a stack of letters indicates the overall site-wise escape metric (as defined in ref.[71]). Letters are colored based on RBD epitope class as indicated in panel a. Right: The overall site-total escape (as defined in ref.[71]) mapped to the surface of a SARS-2 RBD (PDB 6M0J), with white indicating no escape and red indicating escape. Lines with colored numbers according to epitope class indicate RBD positions with the most escape.

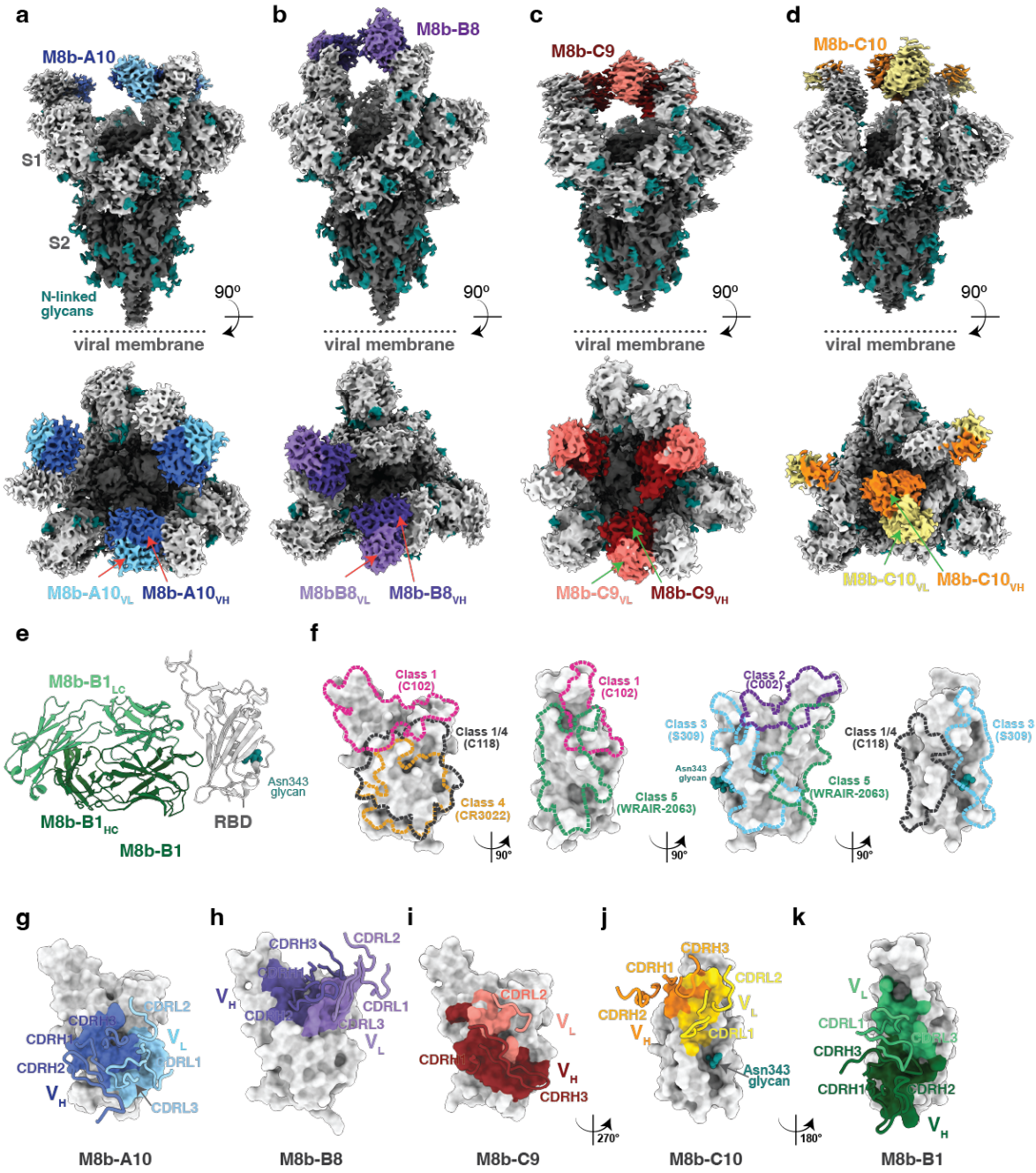

Figure 4. Rabbit mAbs recognize various epitopes on SARS-2 RBDs.
(a-d) Side and top-down views of EM densities of cryo-EM structures of Fab-spike complexes (V_H-V_L densities shown for each Fab) for (a) M8b-A10, (b) M8b-B8, (c) M8b-C9, and (d) M8b-C10. (e) Crystal structure of a M8b-B1 Fab-RBD complex. (f) Epitopes of representative human mAbs from five anti-RBD Ab classes outlined in colored dots using structural information (C102: PDB 7K8M; C002: PDB 7K8T, S309: PDB 7JX3; CR3022: PDB 7LOP; C118: PDB 7RKV; WRAIR-2063: PDB 8EOO). (g-k) Rabbit mAb epitopes with interacting CDRs on a surface representation of SARS-2 RBD (gray) shown as footprints for the indicated V_H and V_L domains for epitopes with superimposed CDR loops for those CDRs that contact the RBD. CDRs were assigned using Kabat definitions[72].

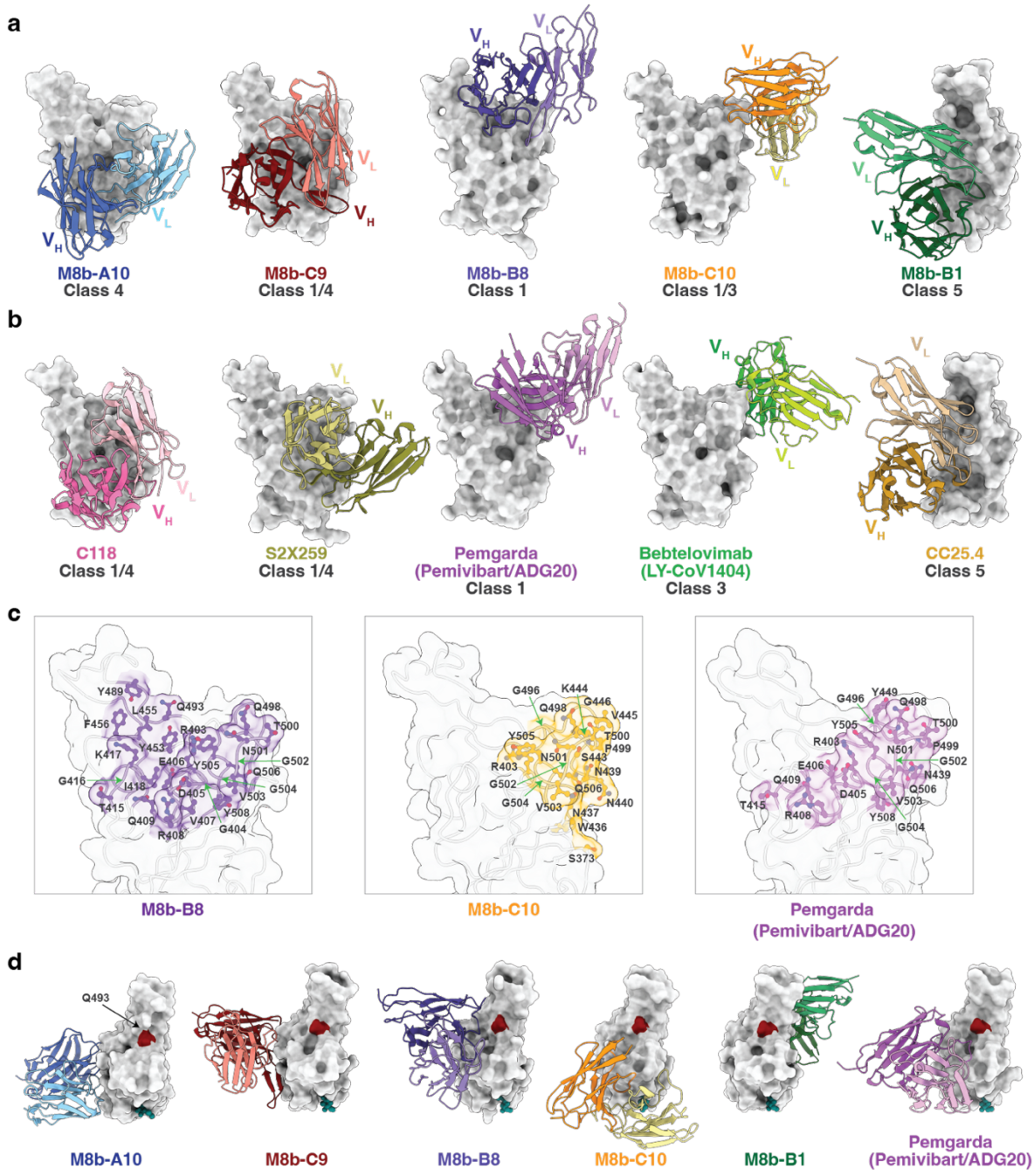

Figure 5. Rabbit and human mAbs recognize similar epitopes.
(a,b) V_H-V_L domains of mAbs (cartoon representations) (rabbit, panel a; human, panel b) complexed with SARS-2 RBD (surface representations). Human anti-RBD mAbs (C118: PDB 7RKV; S2X259: PDB 7M7W; Pemgarda (Pemivibart/ADG20): PDB 7U2D; Bebtelovimab (LY-CoV1404): PDB 7MMO; WRAIR-2063: PDB 8EOO) with similar epitopes are shown below each rabbit mAb-RBD complex. (c) Comparisons of RBD epitopes of selected rabbit mAbs with Pemgarda. RBD epitope residues (determined by PDBePISA[73]) shown as sticks. (d) Comparison of RBD recognition by rabbit mAbs and Pemgarda. The position of RBD residue Q493, which is substituted in recent VOCs that show resistance to Pemgarda[49], is highlighted in dark red.

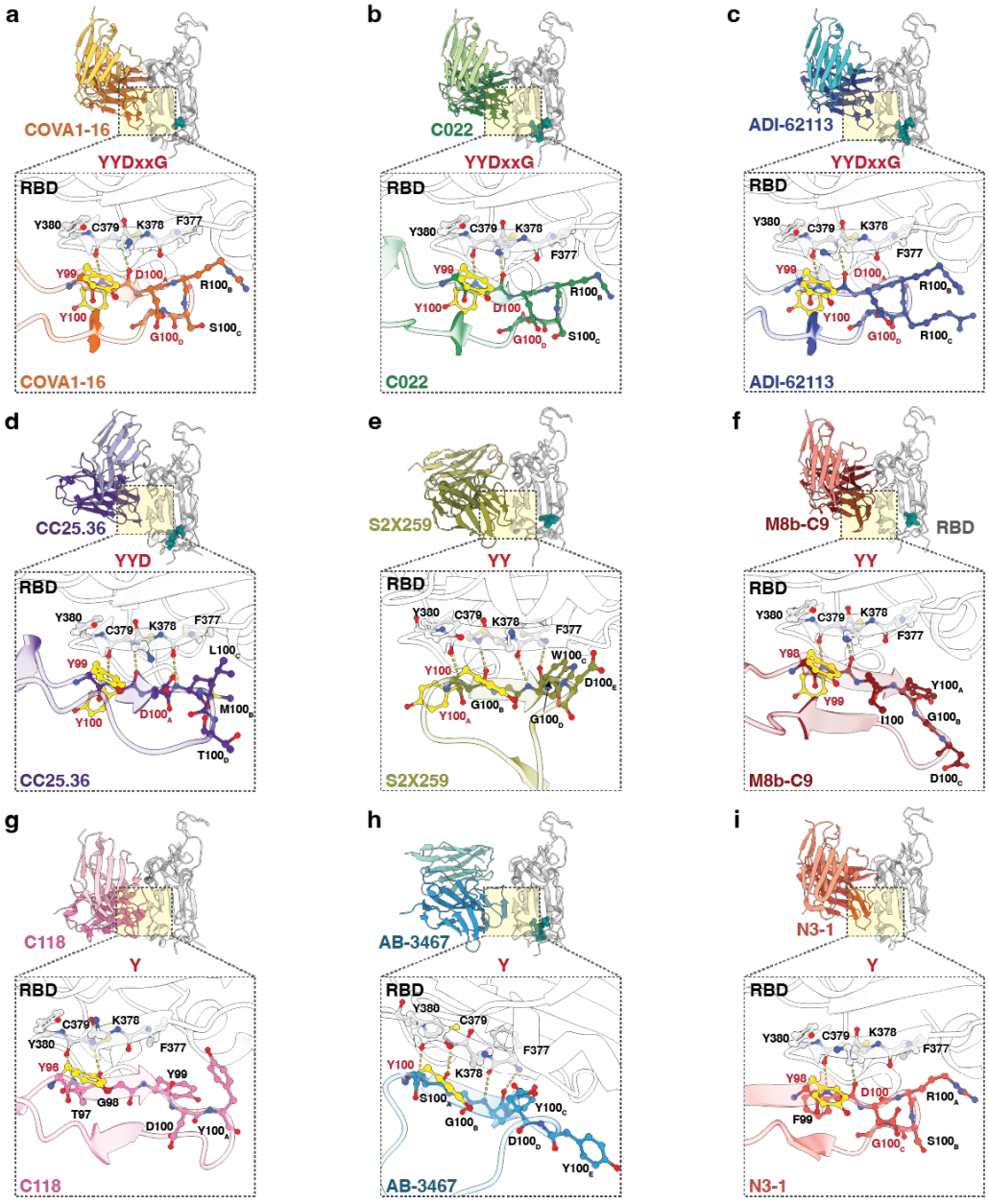

Figure 6. Comparisons of YYDxxG-, YY-, and Y-containing CDRH3 loops in class 1/4 anti-RBD mAbs.

V_H-V_L–RBD complexes (cartoon diagrams) shown for indicated mAbs with zoomed-in insets (yellow shading) showing interactions between mAb CDRH3 loops and RBD as sticks, mainchain hydrogen bonds between a CDRH3 and RBD residues 377-380 as yellow dots, and the sidechains of YY and Y residues within CDRH3 motifs in yellow ball-and-stick representation. RBD (gray) complexes shown for (a) COVA1-16 (PDB 7S5R), (b) C022 (PDB 7RKU), (c) ADI-62113 (PDB 7T7B), (d) CC25.36 (PDB 8SIQ), (e) S2X259 (PDB 7M7W), (f) M8b-C9, (g) C118 (PDB 7RKV), (h) AB-3467 (PDB 7MSQ), and (i) N3-1 (PDB 8TM1). mAb-RBD figures are grouped into YYDxxG, YY, and Y motifs, with names of residues in CDRH3 motifs in red.

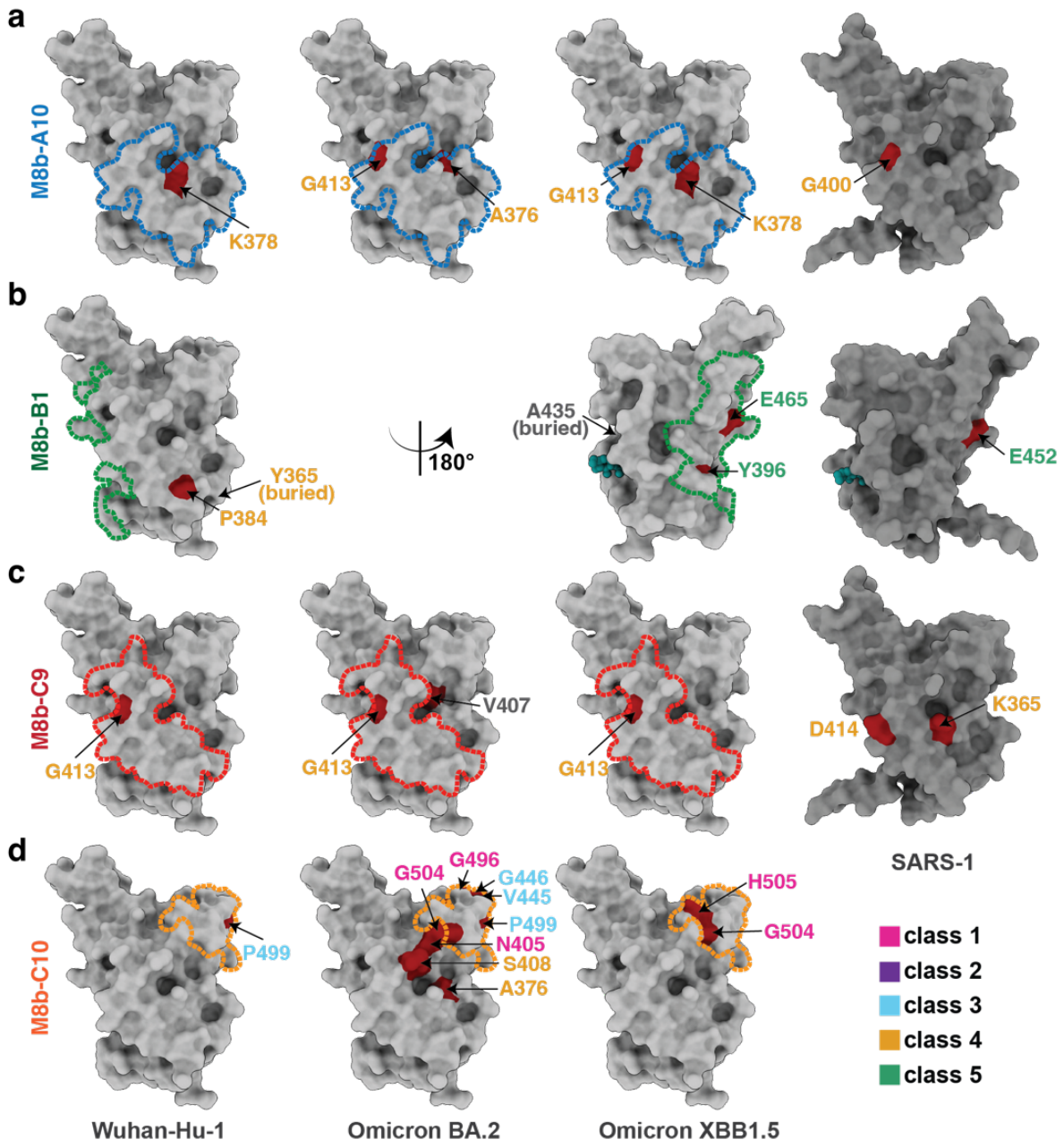

Figure 7. Selection experiments reveal functional escapes.
Positions of residues (highlighted in red on RBD surfaces) in SARS-2 and SARS-1 RBD that were substituted following passage of rVSVs encoding the spike proteins of SARS-2 Wuhan-Hu-1, Omicron BA.2, Omicron XBB.1.5, or SARS-1 with (a) M8b-A10, (b) M8b-B1, (c) M8b-C9, or (d) M8b-C10. Residue names are labeled in colors according to RBD epitope class. Epitopes for these mAbs are outlined in dots colored according to epitope class.

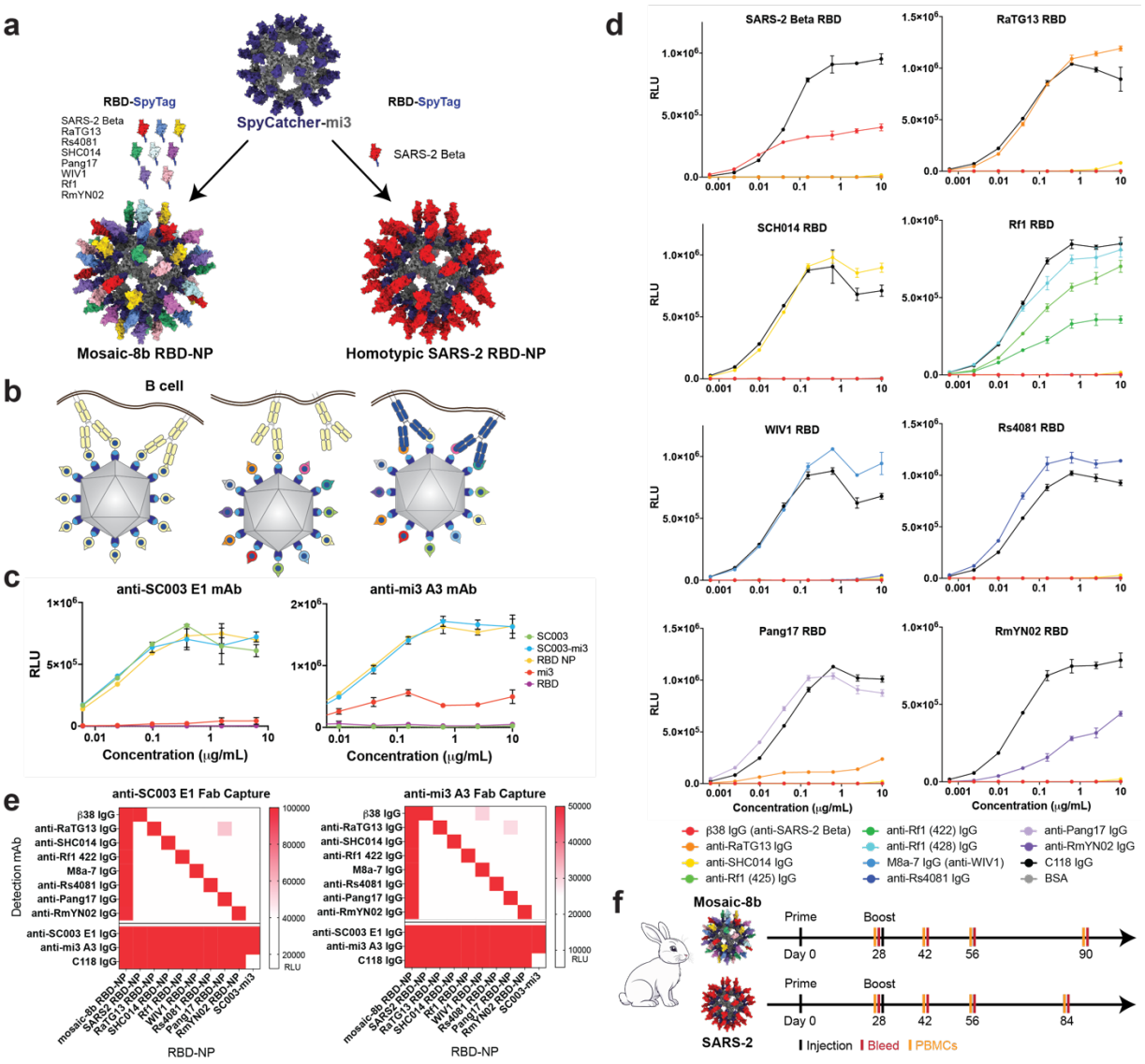

Extended Data Fig. 1. Experimental design for isolation of rabbit mAbs.
(a) Construction of mosaic-8b and homotypic SARS-2 RBD-NPs. Schematic of preparation of mosaic-8b and homotypic SARS-2 RBD-NPs. RBD-NP models were constructed with coordinates of an RBD (PDB 7BZ5), SpyCatcher (PDB 4MLI), and an i3-01 NP (PDB 7B3Y). (b) Hypothesis for preferential elicitation of cross-reactive Abs by mosaic-8b RBD-NPs versus homotypic SARS-2 RBD-NPs. Left: Both Fab arms of a membrane-bound B cell receptor recognizing a strain-specific variable epitope (yellow triangle) can bind to yellow antigens attached to a homotypic RBD-NP. Middle: Only one Fab arm of a B cell receptor recognizing a strain-specific variable epitope (yellow triangle) on a yellow antigen can bind to a mosaic NP when adjacent antigens are different. Right: Both Fab arms of a cross-reactive B cell receptor recognizing a conserved epitope (blue circles) can bind to adjacent antigens on a mosaic NP. (c) Anti-SC003 E1 mAb (left) and anti-mi3 A3 mAb (right) ELISAs of binding to components of NPs (soluble SpyCatcher003, unconjugated SpyCatcher-003 mi3 NPs, RBD-conjugated NPs, mi3, soluble RBD). Anti-SC003 E1 mAb recognizes SpyCatcher003 either as a soluble protein,

attached to mi3 NPs, or on RBD-conjugated NPs. Anti-mi3 A3 mAb recognizes mi3 with and without SpyCatcher and RBD-conjugated NPs. Data are presented as the average of four replicates with error bars representing the standard deviation. (d) ELISAs of 8 anti-RBD mAbs show strain-specific binding to the RBDs present on mosaic-8b RBD-NPs. Data are presented as the average of two replicates with error bars representing the standard deviation. (e) Sandwich ELISA in which mosaic-8 RBD-NPs, each of the 8 homotypic RBD-NPs, and unconjugated SC003-mi3 NPs were captured on an ELISA plate by anti-SC003 E1 (left) or anti-mi3 A3 (right) and detected by strain-specific anti-RBD mAbs. High binding (red) indicates that the RBD corresponding to the mAb is present on the NPs. Low binding (white) indicates the RBD is absent. The human mAb C118 recognizes all 8 RBDs present on the mosaic-8b RBD-NPs[27]. (f) Schematic of immunization regimen. Rabbits received RBD-NP prime and boost immunizations at days 0 and 28. Sera and PBMCs were collected at indicated days. Rabbit clipart from vecteezy.com.

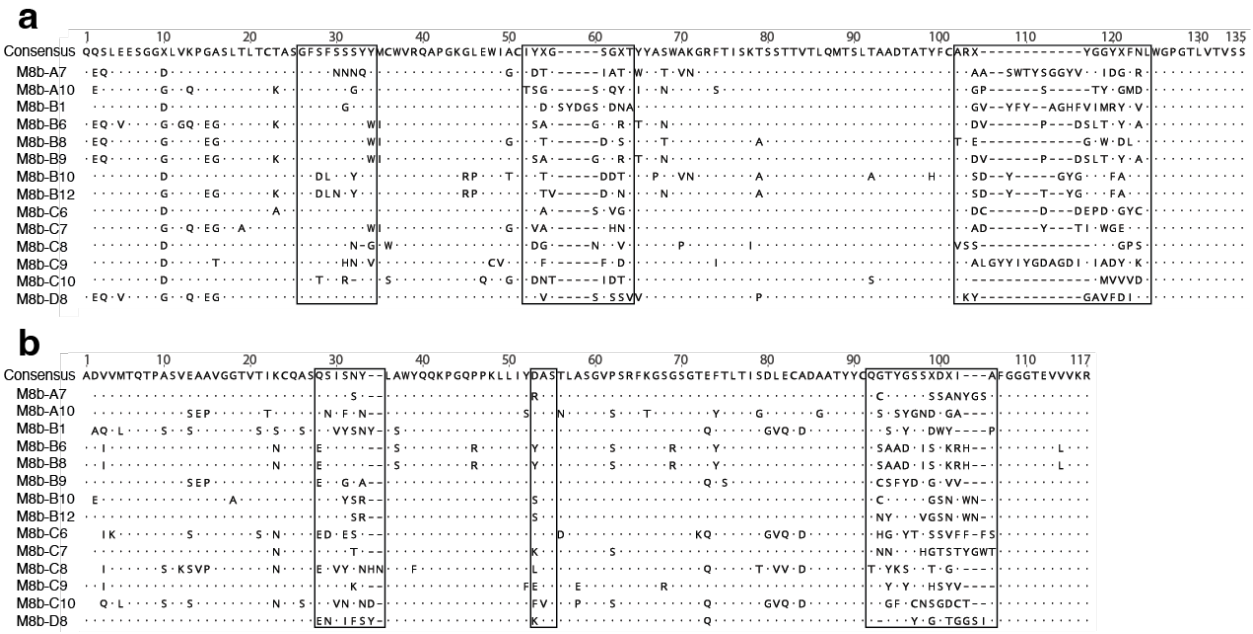

c

	Heavy Chain						Light Chain				
mAb	V-GENE	D-GENE	J-GENE	CDR1 Length	CDR2 Length	CDR3 Length	V-GENE	J-GENE	CDR1 Length	CDR2 Length	CDR3 Length
M8b-A7	IGHV1S40	IGHD6-1	IGHJ4	9	8	21	IGKV1S10	IGKJ1-2	6	3	15
M8b-A10	IGHV1S40	IGHD7-1	IGHJ6	9	9	12	IGKV1S36	IGKJ1-2	6	3	12
M8b-B1	IGHV1S40	IGHD6-1	IGHJ4	9	9	19	IGKV1S15	IGKJ1-2	7	3	11
M8b-B6	IGHV1S45	IGHD1-1	IGHJ4	9	9	14	IGKV1S17	IGKJ1-2	6	3	13
M8b-B8	IGHV1S45	IGHD4-2	IGHJ4	9	8	11	IGKV1S17	IGKJ1-2	6	3	13
M8b-B9	IGHV1S45	IGHD1-1	IGHJ4	9	9	14	IGKV1S36	IGKJ1-2	6	3	12
M8b-B10	IGHV1S40	IGHD6-1	IGHJ4	9	8	16	IGKV1S36	IGKJ1-2	6	3	14
M8b-B12	IGHV1S40	IGHD6-1	IGHJ4	9	8	16	IGKV1S49	IGKJ1-2	6	3	14
M8b-C6	IGHV1S40	IGHD2-1	IGHJ2	9	9	14	IGKV1S47	IGKJ1-2	6	3	14
M8b-C7	IGHV1S45	IGHD4-1	IGHJ4	9	8	14	IGKV1S10	IGKJ1-2	6	3	15
M8b-C8	IGHV1S40	IGHD1-1	IGHJ4	8	9	10	IGKV1S23	IGKJ1-2	8	3	12
M8b-C9	IGHV1S40	IGHD6-1	IGHJ4	9	8	23	IGKV1S10	IGKJ1-2	6	3	11
M8b-C10	IGHV1S40	IGHD7-1	IGHJ4	8	8	9	IGKV1S46 or IGKV1S60	IGKJ1-2	7	3	13
M8b-D8	IGHV1S45	IGHD3-1	IGHJ4	9	9	11	IGKV1S10	IGKJ1-2	6	3	14

d

	A7	A10	B1	B6	B8	B9	B10	B12	C6	C7	C8	C9	C10	D8
A7		71.1	71.2	68.2	72.7	70.5	74	70.1	72.7	70.9	71.9	72.9	73.2	68.2
A10	71.1		73.3	79.3	75	80.2	67.7	72.4	81.8	76	77.3	69.2	74.8	77.5
B1	71.2	73.3		71	70.8	73.3	73.1	71	79.4	74	73.1	77.6	74.6	73.1
B6	68.2	79.3	71		80.3	97.5	64.5	73.2	79.3	81	71.9	68.5	68.6	79.5
B8	72.7	75	70.8	80.3		82.8	73	77.9	77.7	83.3	76.3	69.8	75.2	83.2
B9	70.5	80.2	73.3	97.5	82.8		66.9	75.6	81.8	81.8	74.4	70.8	71.1	78.7
B10	74	67.7	73.1	64.5	73	66.9		86.2	74.2	72.4	72.4	70.5	74.6	69.1
B12	70.1	72.4	71	73.2	77.9	75.6	86.2		74.8	77	71.5	70.5	71.3	73.2
C6	72.7	81.8	79.4	79.3	77.7	81.8	74.2	74.8		80.2	81	75.4	78.5	78.5
C7	70.9	76	74	81	83.3	81.8	72.4	77	80.2		75.2	72.1	75.8	78.5
C8	71.9	77.3	73.1	71.9	76.3	74.4	72.4	71.5	81	75.2		71.5	78.6	73.7
C9	72.9	69.2	77.6	68.5	69.8	70.8	70.5	70.5	75.4	72.1	71.5		70.5	67.7
C10	73.2	74.8	74.6	68.6	75.2	71.1	74.6	71.3	78.5	75.8	78.6	70.5		72
D8	68.2	77.5	73.1	79.5	83.2	78.7	69.1	73.2	78.5	78.5	73.7	67.7	72	

e

	A7	A10	B1	B6	B8	B9	B10	B12	C6	C7	C8	C9	C10	D8
A7		75.4	73.9	80.7	80.7	81.6	90.4	90.4	77	88.6	71.3	86	72.8	85.2
A10	75.4		67	74.1	74.1	80.2	74.3	75.2	67	73.7	69.6	73.9	67.9	74.8
B1	73.9	67		68.1	68.1	74.1	74.6	73.7	77.9	71.3	75.9	75	81.3	72.2
B6	80.7	74.1	68.1		100	77	77	79.8	71.4	80.7	70.8	78.8	70.5	76.7
B8	80.7	74.1	68.1	100		77	77	79.8	71.4	80.7	70.8	78.8	70.5	76.7
B9	81.6	80.2	74.1	77	77		81.4	81.6	75.9	78.1	76.8	80.4	72.3	82.8
B10	90.4	74.3	74.6	77	77	81.4		94.7	74.3	84.2	72.8	83.2	71.7	84.3
B12	90.4	75.2	73.7	79.8	79.8	81.6	94.7		74.3	87.7	72.8	86	72.6	84.5
C6	77	67	77.9	71.4	71.4	75.9	74.3	74.3		73.5	71.1	75	73.5	74.6
C7	88.6	73.7	71.3	80.7	80.7	78.1	84.2	87.7	73.5		69.6	82.5	72.8	82.6
C8	71.3	69.6	75.9	70.8	70.8	76.8	72.8	72.8	71.1	69.6		72.3	74.3	72.2
C9	86	73.9	75	78.8	78.8	80.4	83.2	86	75	82.5	72.3		70.5	79.3
C10	72.8	67.9	81.3	70.5	70.5	72.3	71.7	72.6	73.5	72.8	74.3	70.5		71.1
D8	85.2	74.8	72.2	76.7	76.7	82.8	84.3	84.5	74.6	82.6	72.2	79.3	71.1	

Extended Data Fig. 2. Sequence alignment and identity of VH and VL gene segments from cloned rabbit mAbs. (a,b) Amino acid sequence alignment of 14 rabbit (a) VH and (b) VL gene segments. CDRs (boxed) were identified using IMGT/HighV-Quest[56]. (c) Gene segment usage and CDR lengths were determined for rabbit mAbs using IMGT/HighV-Quest[56]. (d,e) Matrix of percent amino acid identity between rabbit (d) VH and (e) VL gene segments.

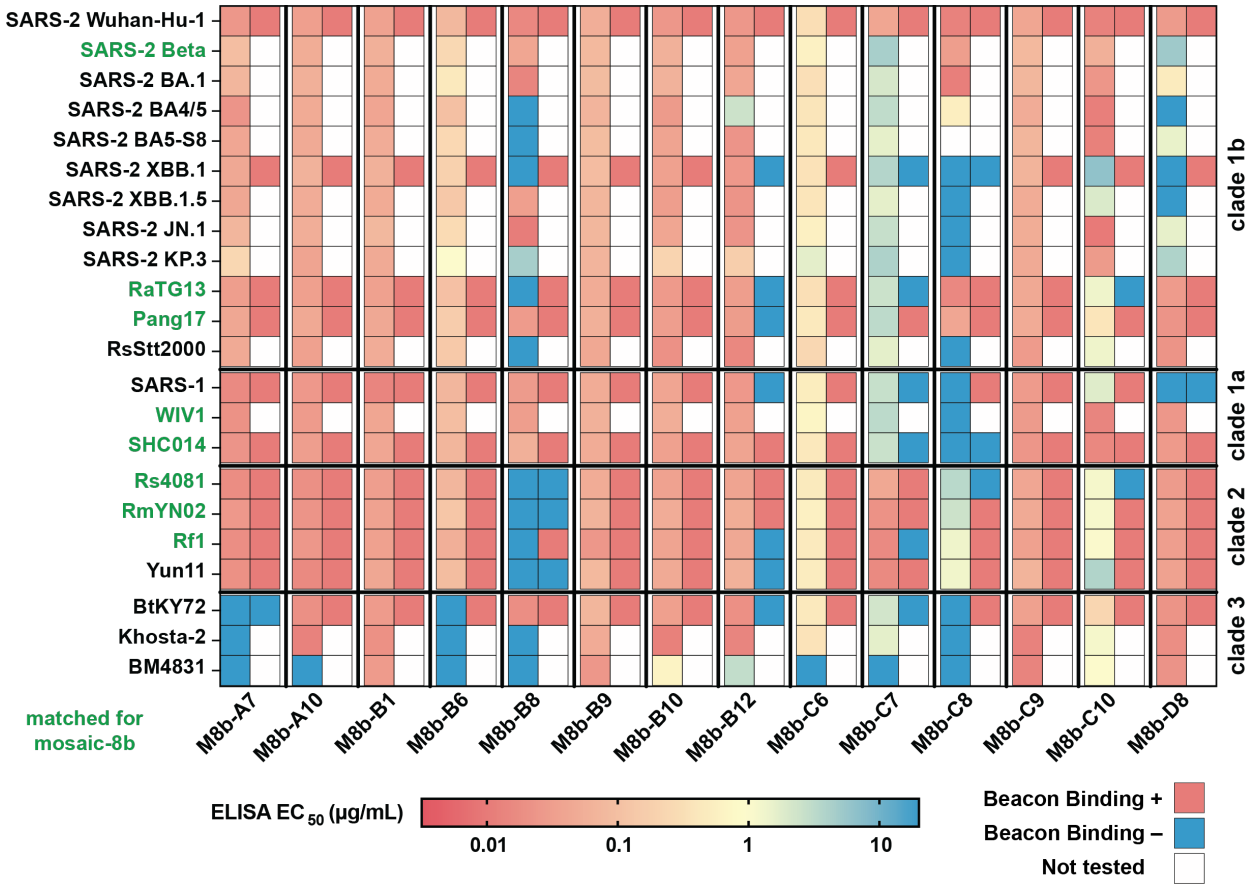

Extended Data Fig. 3. Comparison of ELISA data from recombinantly expressed mAbs and binding data from Beacon multiplexed assays. For each mAb listed at the bottom, ELISA binding is depicted in the column on the left by a color gradient from blue (no binding) to coral (strong binding) for each RBD based on EC_{50} values, and Beacon assay binding is depicted in the column on the right as binding (coral) or no binding (blue) based on detection of a bloom in the multiplexed assays for the indicated RBD. The Beacon multiplexed assays were validated by ELISAs of mAbs, with exceptions including nanopens that contained two cells rather than a single cell (M8b-C8), nanopens in which the signal could retrospectively be assigned to a cell in a neighboring nanopen (M8b-C7), or cells that appear to have died during the assays (M8b-B12).

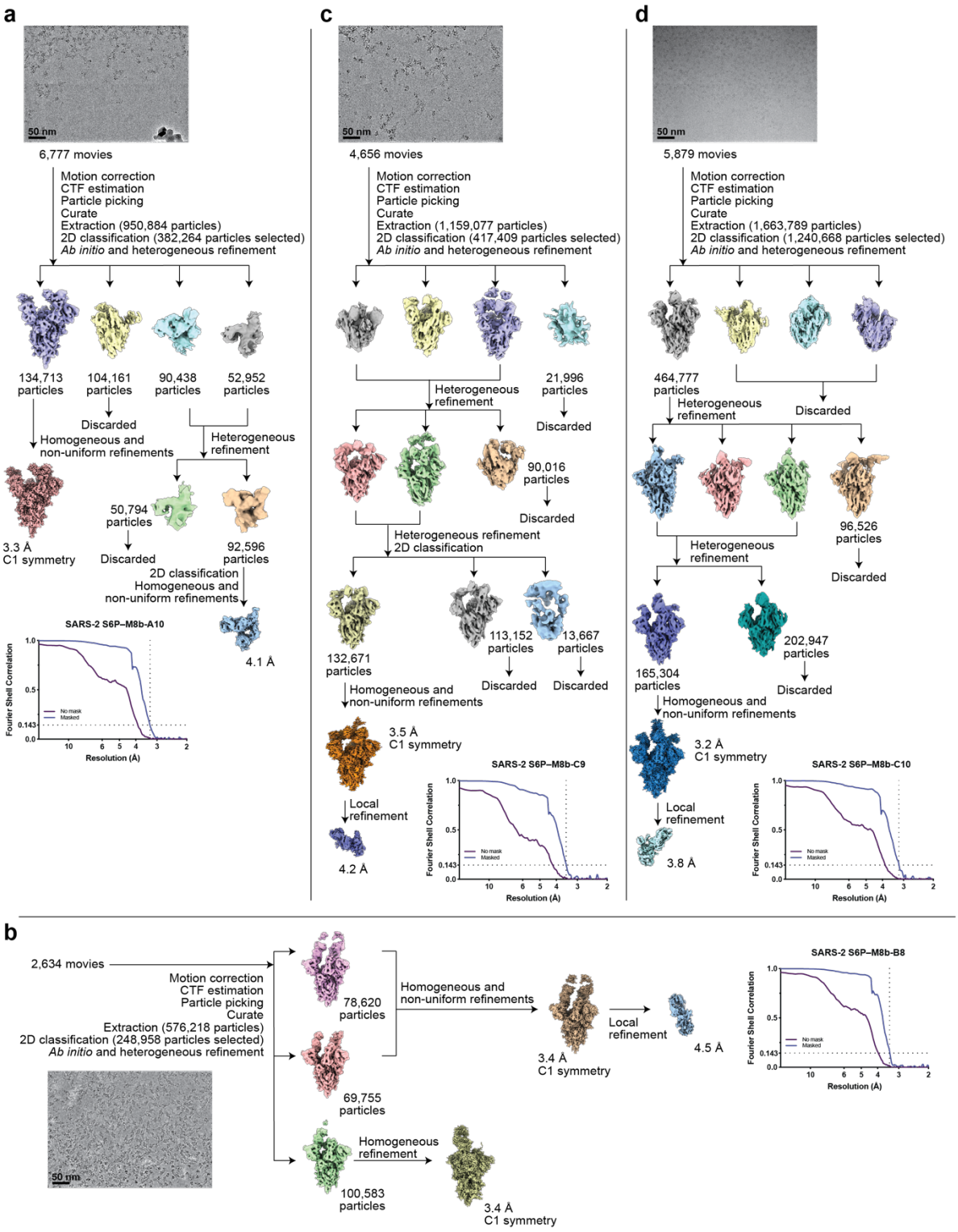

Extended Data Fig. 4. Single-particle cryo-EM processing for SARS-2 spike–mAb complexes. Representative micrographs, workflows for single-particle data processing, and Fourier Shell Correlation plots for final reconstructions are shown for SARS-2 Wuhan-Hu-1 spike complexed with (a) M8b-A10, (b) M8b-B8, (c) M8b-C9, and (d) M8b-C10.

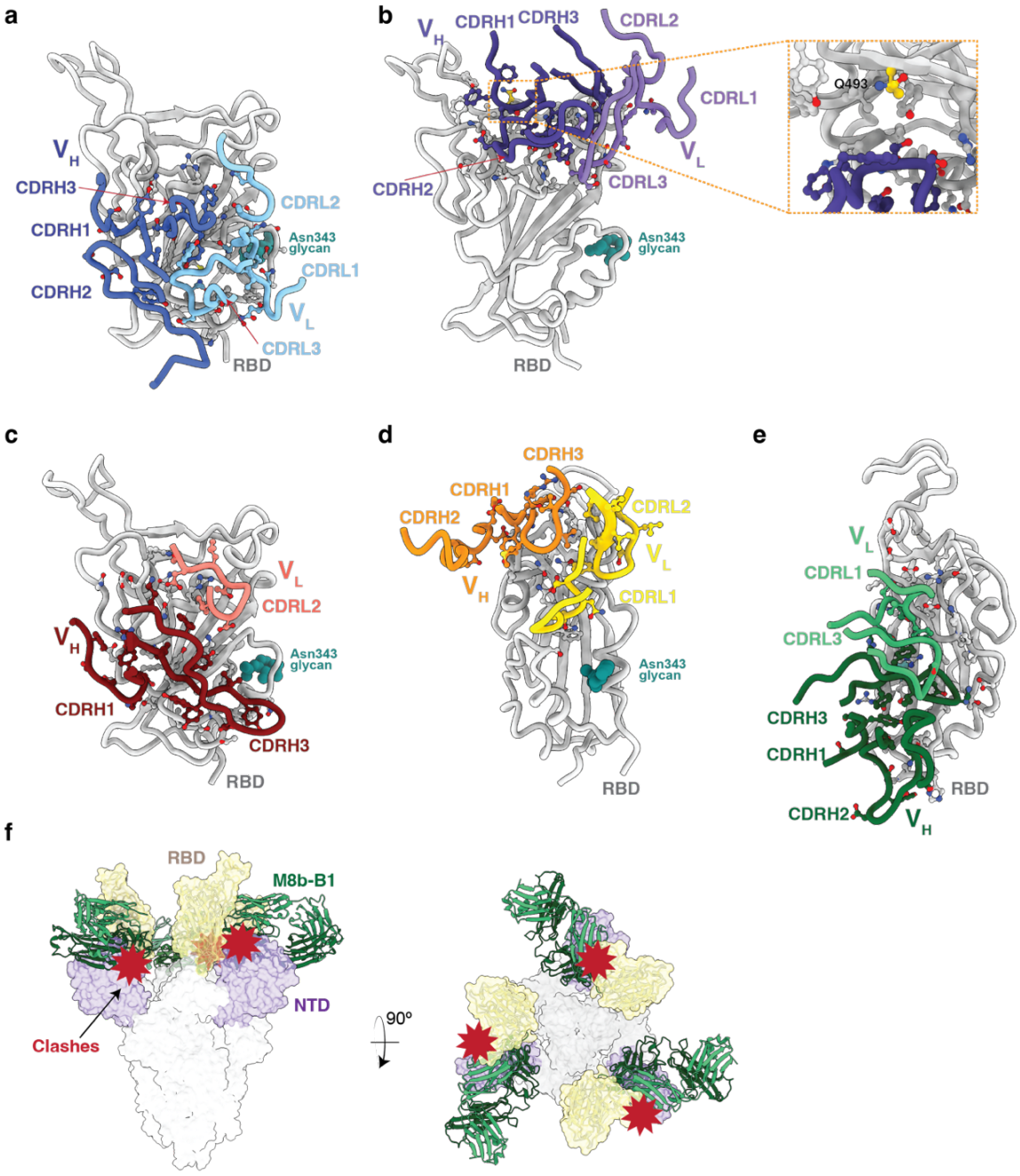

Extended Data Fig. 5. Rabbit mAb recognition of SARS-2 RBD. Interactions are shown between the SARS-2 RBD and RBD-contacting CDRs of (a) M8b-A10, (b) M8b-B8, (c) M8b-C9, (d) M8b-C10, and (e) M8b-B1. RBD residue Q493 is highlighted in yellow in the panel b inset. (f) Modeling of the M8b-B1–RBD structure onto a SARS-2 spike trimer with all "up" RBDs (PDB 7SC1). SARS-2 spike is shown in surface representation with yellow RBDs and purple N-terminal domains (NTDs). The RBD portion of the M8bB1–RBD coordinates (cartoon representation; green M8b-B1 Fab, yellow RBD) was aligned on the RBDs of the spike trimer structure. Steric clashes between the M8b-B1 Fab and the spike NTD are highlighted as red bursts.

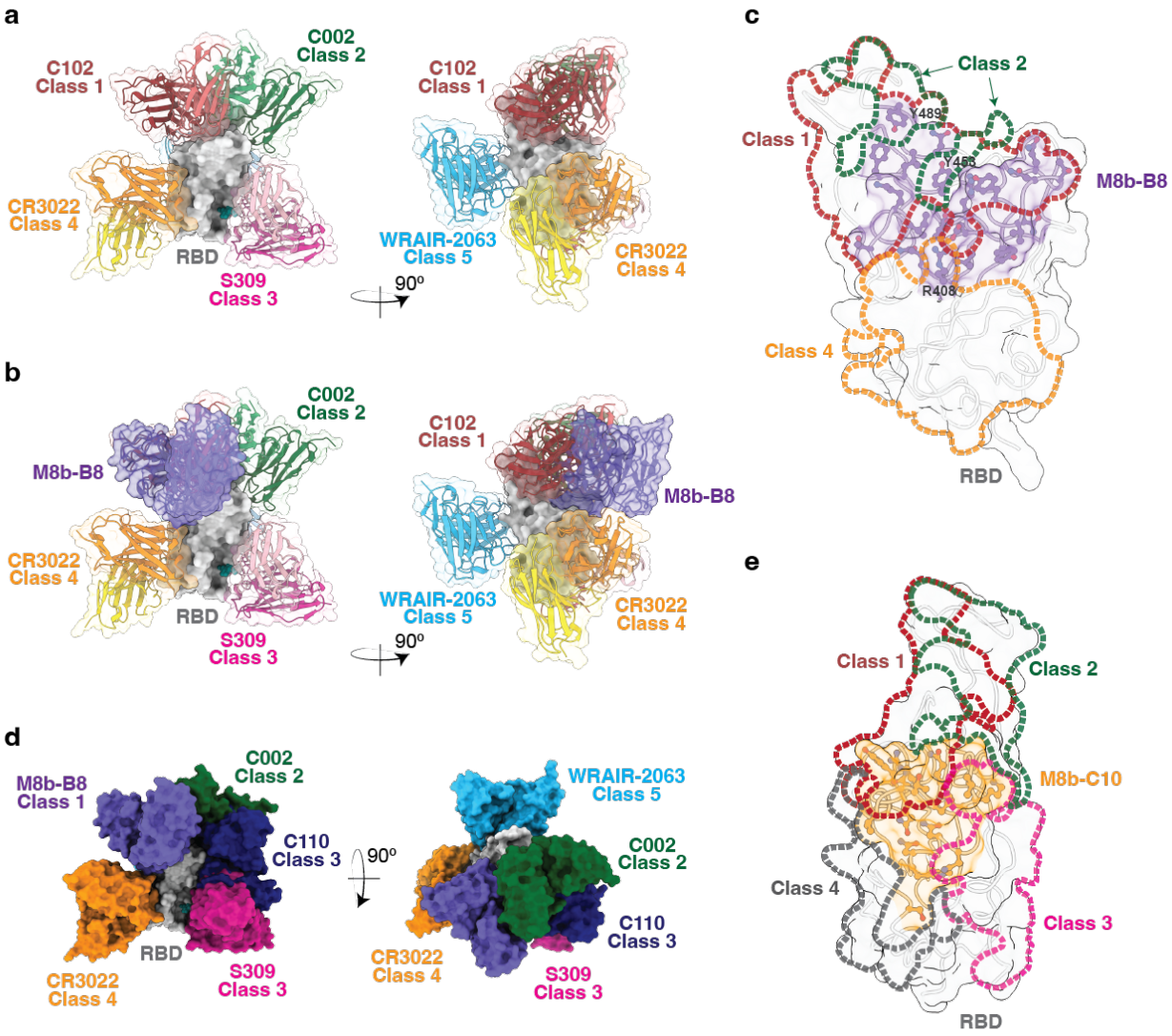

Extended Data Fig. 6. Epitope classifications of M8b-B8 and M8b-C10. (a) V_H-V_L domains of representative mAbs recognizing previously-defined RBD epitopes[22,29,30]: C102: PDB 7K8M; C002: PDB 7K8T, S309: PDB 7JX3; CR3022: PDB 7LOP; WRAIR-2063: PDB 8EOO. (b) Overlap of the binding footprints of M8b-B8 (purple RBD residues), C102 (class 1, red dotted outline), C002 (class 2, green dotted outline), and CR3022 (class 4, orange dotted outline). (c) The M8b-B8 epitope (light purple) primarily overlaps with the class 1 RBD epitope (exemplified by C102; red dotted line). Two residues within the M8b-B8 epitope (Y453 and Y489) overlap with the class 2 RBD epitope (exemplified by C002; green dotted line), and one residue (Y408) overlaps with the class 4 RBD epitope (exemplified by CR3022; orange dotted line). (d) Composite model showing that binding of M8b-B8 could sterically interfere with the binding of the class 2 mAb C002, the class 3 mAb C110, and the class 4 mAb CR3022. (e) The epitope of M8b-C10 (orange) primarily overlaps with the class 1 RBD epitope (exemplified by C102; red dotted lines) and the class 3 RBD epitope (exemplified by S309; magenta dotted line).

Extended Data Table 1. V_H and V_L sequences of anti-NP and strain-specific anti-RBD mAbs.

mAb Name	VH/VL Origin	VH nucleotide sequence	VH amino acid sequence	VL nucleotide sequence	VL amino acid sequence	Reference
anti-SC003 E1 IgG	Rabbit	CAGCAGCTGGAGCAGTCCGAGGGAGACCTGGTCAAGCCTGGGGCATCCCTGACACTCTCCTGCAAAGCCTCTGGATTCTCCTTCAGTGGCAATGTTATGTGCTGGGTCCGCCAGGCTCCAGGGAAGGGGCTGGAGTGGATCGGATGCATTTATATTGTTGATGGCAAGACTTACTACGCGAGCTGGGTGAATGGCCGATTCACCATCTCCAAAACCTCGTCGACCACGGTGACTCTGCAAATGACCAGTCTGACAGCCGCGGACACGGCCACCTATTTCTGTGCGAGGGGGACTTATGCTGGTTATGGTGGTGGTGGTGATCTCTTTGACGAGTTTAATTTGTGGGGCCCCGGCACCCCGGTCACCGTCTCCTCA	QQLEQSEGDLVKPGASLTLSCKASGFSFSGNVMCWVRQAPGKGLEWIGCIYIVDGKTYYASWVNGRFTISKTSSTTVTLQMTSLTAADTATYFCARGTYAGYGGGGDLFDEFNLWGPGTPVTVSS	GCCCTTGTGATGACCCAGACTCCAGCCTCCGTGTCTGAACCTGTGGGAGGCACAGTCACCGTCAAGTGCCAGGCCAGTGAGAACATTTATAGCAATTTAGCCTGGTATCAGCAGAAACCAGGGCAGCCTCCCAAGCTCCTGATCTACAAGGCATCCACTCTGGCATCTGGGGTCCCATCGCGGTTCAAAGGCAGTGGATCTCGGACAGAGTACACTCTCACCATCAGCGACCTGGAGTGTGCCGATGCTGCCACTTACTACTGTCAAAGCAATTTTGGTGGTACTAGTATGAGTTATTATTTCGGCGGATGGACCGAGGTGGTGGTCAAACGT	ALVMTQTPASVSEPVGGTVTVKCQASENIYSNLAWYQQKPGQPPKLLIYKASTLASGVPSRFKGSGSRTEYTLTISDLECADAATYYCQSNFGGTSMSYYFGGWTEVVVKR	This paper
anti-mi3 A3 IgG	Human	CAGCAGCTGGAGCAGTCCGGGGGAGGCCTGGTCCAGCCTGAGGGATCCCTGACACTCACCTGCAAAGCCTCTGGAATCGACTTCAGTAGCTACTACTACATGTGCTGGGTCCGCCAGGCTCCAGGGAAGGGGCTGGAGTTGATCGGATGCATTAATACTGGTGGTAATGGTGCCACTTACTACGCGAGCTGGGCGAAAGGCCGATTCACCATCTCCAGAACCTCGTCGACCACGGTGACTCTGCAAATGACCAGTTTGACAGCCGCGGACACGGCCACCTATTTCTGTGCGAGAGATCTCTATTATAATGTTGGTAACTATGGGGGCTTGTGGGGCCCAGGCACCCTGGTCACCGTCTCCTCA	QQLEQSGGGLVQPEGSLTLTCKASGIDFSSYYYMCWVRQAPGKGLELIGCINTGGNGATYYASWAKGRFTISRTSSTTVTLQMTSLTAADTATYFCARDLYYNVGNYGGLWGPGTLVTVSS	GCCCTTGTGATGACCCAGACTCCAGCCTCCGTGTCTGCCGCTGTGGGAGGCACAGTCACCATCAAGTGCCAGGCCAGTCAGAACATTAAGAACCAACTATCCTGGTATCAACAGAAACCAGGGCAGCGTCCCAAGCTCCTGGTCTACGATGCATCCGAACTGGCATCTGGGGTCCCATCACGGTTCGGTGGCAGTGGATCTGGGACAGAGTACACTCTCGCCATCAGCGACCTGGAGTGTGCCGATGCTGCCACTTACTACTGTCAACAGGGTTGGAATATTGATGGGGTTGATAATGTTTTCGGCGGAGGGACCGAGGTGGTGGTCAAA	ALVMTQTPASVSAAVGGTVTIKCQASQNIKNQLSWYQQKPGQRPKLLVYDASELASGVPSRFGGSGSGTEYTLAISDLECADAATYYCQQGWNIDGVDNVFGGGTEVVVK	This paper
Beta-38 IgG	Human	GAAGTGCAGCTGGTTCAGTCTGGCGCCGAAGTGAAGAAGCCTGGCGAGAGCCTGAAGATCAGCTGCAAAGGCAGCGGCTACAGCTTCACCAACTACTGGATCGGCTGGGTCCGACAGATGCCTGGCAAAGGCCTTGAGTGGATGGGCATCATCTACCCCGGCGATAGCGGCACCAGATACAGCCCTAGCTTTCAGGGCCAAGTGACCATCAGCGCCGACAAGAGCATCAGAACCGCCTACCTGCAGTGGTCCAGCCTGAAGGCCTCTGACAGCGCCATGTACTACTGCGCCAGATCTAGAGTGGGAGCCACCGGCGGCTACTACGACTACTACATGGATGTGTGGGGCCAGGGCACCACCGTGACAGTTTCTTCT	EVQLVQSGAEVKKPGESLKISCKGSGYSFTNYWIGWVRQMPGKGLEWMGIIYPGDSGTRYSPSFQGQVTISADKSIRTAYLQWSSLKASDSAMYYCARSRVGATGGYYDYYMDVWGQGTTVTVSS	CAGTCTGTGCTGACACAGCCTCCATCTGCCTCTGGCACACCTGGCCAGAGAGTGACCATCAGCTGTAGCGGCAGCAGCAGCAATCTCGGCGGCAACACCGTGAACTGGTATCAGCAGCTGCCTGGCACAGCCCCTAAACTGCTGATCTACAGCAACAACCAGCGGCCTAGCGGCGTGCCCGATAGATTTTCTGGCAGCAAGAGCGGCACAAGCGCCAGCCTGGCTATTTCTGGACTGCAGAGCGAGGACGAGGCCGACTATTATTGTGCCGCCTGGGACGACAGCCTGAACGGCCCTGTTTTTGGCACCGGCACCAAAGTGACAGTGCTG	QSVLTQPPSASGTPGQRVTISCSGSSSNLGGNTVNWYQQLPGTAPKLLIYSNNQRPSGVPDRFSGSKSGTSASLAISGLQSEDEADYYCAAWDDSLNGPVFGTGTKVTVL	Liu et al., Cell Host & Microbe, 2022
anti-Pang17 IgG	Human	CAGGTGCAATTGGTGCAGAGCGGTGCCGAAGTGAAAAAACCGGGCAGCAGCGTGAAAGTTAGCTGCAAAGCATCCGGAGGGACGTTTAACGACTACGCTATGTCTTGGGTGCGCCAGGCCCCTGGACAGGGCCTCGAGTGGATGGGCGGTATCATCCCGAAATTCGGCACTGCGTACTACGCCCAGAAATTTCAGGGCCGGGTGACCATTACCGCCGATGAAAGCACCAGCACCGCCTATATGGAACTGAGCAGCCTGCGCAGCGAAGATACGGCCGTGTATTATTGCGCGCGTGGTCCGGCTGTTGGTTACCCGTCTAACATCTACTACGAATACCCGTACGATGTTTGGGGCCAAGGCACCCTGGTGACTGTTAGCTCA	QVQLVQSGAEVKKPGSSVKVSCKASGGTFNDYAMSWVRQAPGQGLEWMGGIIPKFGTAYYAQKFQGRVTITADESTSTAYMELSSLRSEDTAVYYCARGPAVGYPSNIYYEYPYDVWGQGTLVTVSS	GATATCCAGATGACCCAGAGCCCGAGCAGCCTGAGCGCCAGCGTGGGCGATCGCGTGACCATTACCTGCAGAGCCAGCCAGGACATTTCTAACCGTCTGGCTTGGTACCAGCAGAAACCGGGCAAAGCGCCGAAACTATTAATCTACGCTGCTTCTAACCTGCAAAGCGGCGTGCCGAGCCGCTTTAGCGGCAGCGGATCCGGCACCGATTTCACCCTGACCATTAGCTCTCTGCAACCGGAAGACTTTGCGACCTATTATTGCCATCAGTACTACTCTACTCCGCCGACCTTTGGCCAGGGCACGAAAGTTGAAATTAAA	DIQMTQSPSSLSASVGDRVTITCRASQDISNRLAWYQQKPGKAPKLLIYAASNLQSGVPSRFSGSGSGTDFTLTISSLQPEDFATYYCHQYYSTPPTFGQGTKVEIK	This paper
anti-Rf1422 IgG	Human	GAAGTGCAATTGCTGGAAAGCGGCGGTGGCCTGGTGCAGCCGGGTGGCAGCCTGCGTCTGAGCTGCGCGGCGTCCGGATTCACCTTTTCTTCTGCTGCTATGCATTGGGTGCGCCAGGCCCCGGGCAAAGGTCTCGAGTGGGTTTCCTCTATCTCTTACTACGGTTCTTCTACCGACTATGCGGATAGCGTGAAAGGCCGCTTTACCATCAGCCGCGATAATTCGAAAAACACCCTGTATCTGCAAATGAACAGCCTGCGTGCGGAAGATACGGCCGTGTATTATTGCGCGCGTAACTTCCCGGGTTACGGTGCTTACTACATGGATTACTGGGGCCAAGGCACCCTGGTGACTGTTAGCTCA	EVQLLESGGGLVQPGGSLRLSCAASGFTFSSAAMHWVRQAPGKGLEWVSSISYYGSSTDYADSVKGRFTISRDNSKNTLYLQMNSLRAEDTAVYYCARNFPGYGAYYMDYWGQGTLVTVSS	GATATCCAGATGACCCAGAGCCCGAGCAGCCTGAGCGCCAGCGTGGGCGATCGCGTGACCATTACCTGCAGAGCCAGCCAGTCTATTGGTGACTACCTGAACTGGTACCAGCAGAAACCGGGCAAAGCGCCGAAACTATTAATCTACGCTGCTTCTTCTCTGCAAAGCGGCGTGCCGAGCCGCTTTAGCGGCAGCGGATCCGGCACCGATTTCACCCTGACCATTAGCTCTCTGCAACCGGAAGACTTTGCGACCTATTATTGCCAGCAGGCTTACTTCACTCCGCTGACCTTTGGCCAGGGCACGAAAGTTGAAATTAAA	DIQMTQSPSSLSASVGDRVTITCRASQSIGDYLNWYQQKPGKAPKLLIYAASSLQSGVPSRFSGSGSGTDFTLTISSLQPEDFATYYCQQAYFTPLTFGQGTKVEIK	This paper
anti-Rf1425 IgG	Human	CAGGTGCAATTGGTGCAGAGCGGTGCCGAAGTGAAAAAACCGGGCAGCAGCGTGAAAGTTAGCTGCAAAGCATCCGGAGGGACGTTTTCTGACTACGCTATCTCTTGGGTGCGCCAGGCCCCTGGACAGGGCCTCGAGTGGATGGGCCGTATCTACCCGATCTTCGGCACTGCGAACTACGCCCAGAAATTTCAGGGCCGGGTGACCATTACCGCCGATGAAAGCACCAGCACCGCCTATATGGAACTGAGCAGCCTGCGCAGCGAAGATACGGCCGTGTATTATTGCGCGCGTGAACAGTACTACTCTTCTTCTATCGGTTTCGATTACTGGGGCCAAGGCACCCTGGTGACTGTTAGCTCA	QVQLVQSGAEVKKPGSSVKVSCKASGGTFSDYAISWVRQAPGQGLEWMGRIYPIFGTANYAQKFQGRVTITADESTSTAYMELSSLRSEDTAVYYCAREQYYSSSIGFDYWGQGTLVTVSS	GATATCGAACTGACCCAGCCGCCGAGCGTGAGCGTGAGCCCGGGCCAGACAGCTAGCATTACCTGTAGCGGCGATAAAATCCCGAAAAAAGCTGTTCATTGGTACCAGCAGAAACCGGGCCAGGCGCCGGTGCTGGTGATCTACGACGACAACGACCGTCCGAGCGGCATCCCGGAACGTTTTAGCGGATCCAACAGCGGCAACACCGCGACCCTGACCATTAGCGGCACCCAGGCGGAAGACGAAGCGGATTATTACTGCGCTTCTTGGGACCTGGGTTCTTACGTGTTTGGCGGCGGCACGAAGTTAACCGTTCTT	DIELTQPPSVSVSPGQTASITCSGDKIPKKAVHWYQQKPGQAPVLVIYDDNDRPSGIPERFSGSNSGNTATLTISGTQAEDEADYYCASWDLGSYVFGGGTKLTVL	This paper
anti-Rf1428 IgG	Human	CAGGTGCAATTGGTGCAGAGCGGTGCCGAAGTGAAAAAACCGGGCAGCAGCGTGAAAGTTAGCTGCAAAGCATCCGGAGGGACGTTTTCTTCTTACGCTATCTCTTGGGTGCGCCAGGCCCCTGGACAGGGCCTCGAGTGGATGGGCGGTATCGTTCCGATCTTCGGCGCTGCGACTTACGCCCAGAAATTTCAGGGCCGGGTGACCATTACCGCCGATGAAAGCACCAGCACCGCCTATATGGAACTGAGCAGCCTGCGCAGCGAAGATACGGCCGTGTATTATTGCGCGCGTGACCTGCATTACTACGCTATCGATGTTTGGGGCCAAGGCACCCTGGTGACTGTTAGCTCA	QVQLVQSGAEVKKPGSSVKVSCKASGGTFSSYAISWVRQAPGQGLEWMGGIVPIFGAATYAQKFQGRVTITADESTSTAYMELSSLRSEDTAVYYCARDLHYYAIDVWGQGTLVTVSS	GATATCCAGATGACCCAGAGCCCGAGCAGCCTGAGCGCCAGCGTGGGCGATCGCGTGACCATTACCTGCAGAGCCAGCCAGGACATTATCACTTACCTGGCTTGGTACCAGCAGAAACCGGGCAAAGCGCCGAAACTATTAATCTACGCTGCTTCTACTCTGCAAAGCGGCGTGCCGAGCCGCTTTAGCGGCAGCGGATCCGGCACCGATTTCACCCTGACCATTAGCTCTCTGCAACCGGAAGACTTTGCGACCTATTATTGCCAGCAGTACGACCAGGGTCCGATCACCTTTGGCCAGGGCACGAAAGTTGAAATTAAA	DIQMTQSPSSLSASVGDRVTITCRASQDIITYLAWYQQKPGKAPKLLIYAASTLQSGVPSRFSGSGSGTDFTLTISSLQPEDFATYYCQQYDQGPITFGQGTKVEIK	This paper
anti-RmYN02 IgG	Human	CAGGTGCAATTGGTGCAGAGCGGTGCCGAAGTGAAAAAACCGGGCAGCAGCGTGAAAGTTAGCTGCAAAGCATCCGGAGGGACGTTTAACTCTTACTCTATCTCTTGGGTGCGCCAGGCCCCTGGACAGGGCCTCGAGTGGATGGGCGGTATCATCCCGATCTTCGGCACTGCGAACTACGCCCAGAAATTTCAGGGCCGGGTGACCATTACCGCCGATGAAAGCACCAGCACCGCCTATATGGAACTGAGCAGCCTGCGCAGCGAAGATACGGCCGTGTATTATTGCGCGCGTGACCTGGTTGACAACGCTGTTTCTATGTACCCGCTGGATCCGTGGGGCCAAGGCACCCTGGTGACTGTTAGCTCA	QVQLVQSGAEVKKPGSSVKVSCKASGGTFNSYSISWVRQAPGQGLEWMGGIIPIFGTANYAQKFQGRVTITADESTSTAYMELSSLRSEDTAVYYCARDLVDNAVSMYPLDPWGQGTLVTVSS	GATATCCAGATGACCCAGAGCCCGAGCAGCCTGAGCGCCAGCGTGGGCGATCGCGTGACCATTACCTGCAGAGCCAGCCAGGACATTCGTAACTACCTGGCTTGGTACCAGCAGAAACCGGGCAAAGCGCCGAAACTATTAATCTACGACGCTTCTAACCTGCAAAGCGGCGTGCCGAGCCGCTTTAGCGGCAGCGGATCCGGCACCGATTTCACCCTGACCATTAGCTCTCTGCAACCGGAAGACTTTGCGACCTATTATTGCCAGCAGTACGGTGCTACTTCTTACACCTTTGGCCAGGGCACGAAAGTTGAAATCAAA	DIQMTQSPSSLSASVGDRVTITCRASQDIRNYLAWYQQKPGKAPKLLIYDASNLQSGVPSRFSGSGSGTDFTLTISSLQPEDFATYYCQQYGATSYTFGQGTKVEIK	This paper
anti-Rs4081 IgG	Human	GAAGTGCAATTGGTGGAAAGCGGCGGTGGCCTGGTGAAACCAGGCGGCAGCCTGCGCCTGAGCTGCGCCGCCTCCGGATTCACCTTTAACTCTTACGCTCTGCATTGGGTGCGCCAGGCCCCGGGCAAAGGTCTCGAGTGGGTGGGCCGTATCCGTTCTAAAACTGACGGTGGTACTACTCATTATGCCGCCCCAGTGAAAGGCCGCTTTACCATTAGCCGCGATGATTCGAAAAACACCCTGTATCTGCAAATGAACAGCCTGAAAACCGAAGATACGGCCGTGTATTATTGCGCGCGTGGTGGTCTGTACGACTACTACTACGACTACTTCGATTACTGGGGCCAAGGCACCCTGGTGACTGTTAGCTCA	EVQLVESGGGLVKPGGSLRLSCAASGFTFNSYALHWVRQAPGKGLEWVGRIRSKTDGGTTHYAAPVKGRFTISRDDSKNTLYLQMNSLKTEDTAVYYCARGGLYDYYYDYFDYWGQGTLVTVSS	GATATCGTGCTGACCCAGCCGCCGAGCGTGAGCGGTGCACCGGGACAGCGAGTGACCATTAGCTGTAGCGGCAGCAGCAGCAACATTGGTATCAACACTGTGAACTGGTACCAGCAGCTGCCGGGCACGGCGCCGAAAGTTCTGATCTACTCTAACTCTCATCGCCCGAGCGGCGTGCCGGATCGCTTTAGCGGATCCAAAAGCGGCACCAGCGCCAGCCTGGCGATTACCGGCCTGCAAGCAGAAGACGAAGCGGATTATTACTGCTCTTCTACTGCTGAACTGGACTCTGGTTGGGTGTTTGGCGGCGGCACGAAGTTAACCGTTCTT	DIVLTQPPSVSGAPGQRVTISCSGSSSNIGINTVNWYQQLPGTAPKVLIYSNSHRPSGVPDRFSGSKSGTSASLAITGLQAEDEADYYCSSTAELDSGWVFGGGTKLTVL	This paper
anti-SCH014 IgG	Human	CAGGTGCAATTGGTGCAGAGCGGTGCCGAAGTGAAAAAACCGGGCAGCAGCGTGAAAGTTAGCTGCAAAGCATCCGGAGGGACGTTTTCTTCTTACGCTATCTCTTGGGTGCGCCAGGCCCCTGGACAGGGCCTCGAGTGGATGGGCGGTATCATCCCGGTTTTCGGCGAAGCGAACTACGCCCAGAAATTTCAGGGCCGGGTGACCATTACCGCCGATGAAAGCACCAGCACCGCCTATATGGAACTGAGCAGCCTGCGCAGCGAAGATACGGCCGTGTATTATTGCGCGCGTATGGGTTGGTGGGACTTCTGGGGCCAAGGCACCCTGGTGACTGTTAGCTCA	QVQLVQSGAEVKKPGSSVKVSCKASGGTFSSYAISWVRQAPGQGLEWMGGIIPVFGEANYAQKFQGRVTITADESTSTAYMELSSLRSEDTAVYYCARMGWWDFWGQGTLVTVSS	GATATCGAACTGACCCAGCCACCGAGCGTGAGCGTGAGCCCGGGCCAGACCGCGAGCATTACCTGTAGCGGCGATAACATCGGTCAGAAATCTTACAACTGGTACCAGCAGAAACCGGGCCAGGCGCCGGTGCTGGTGATCTACGACAACGACGACCGTCCGAGCGGCATCCCGGAACGTTTTAGCGGATCCAACAGCGGCAACACCGCGACCCTGACCATTAGCGGCACCCAGGCGGAAGACGAAGCGGATTATTACTGCCAGTCTTGGACTTGGTCTTGGCTGTCTTACGTGTTTGGCGGCGGCACGAAGTTAACCGTTCTT	DIELTQPPSVSVSPGQTASITCSGDNIGQKSYNWYQQKPGQAPVLVIYDNDDRPSGIPERFSGSNSGNTATLTISGTQAEDEADYYCQSWTWSWLSYVFGGGTKLTVL	This paper
anti-RaTG13 F1	Rabbit	CAGCAGCTGGAGCAGTCCGGGGGAGGCCTGGTCCAGCCTGAGGGATCCCTGACACTCACCTGCACAGTCTCTGGATTCTCGTGGAAGTACGATTACATGTGCTGGGTCCGCCAGGCTCCAGGGAAGGGGCTGGAGTGGATCGTATGTATTTATGGTGATAGTGGTAGCACATGGTACGCGAGCTGGGTGAATGGCCGATTCACCATTTCCAAAACCTCGTCGACCACGGTGACTCTGCAAATGGCTAGTCTGACAGTCGCGGACACGGCCACCTATTTCTGTGCGAGAGCCGATACTGGTGCTGGTGGTTACCCGTTTAACTTGTGGGGCCCAGGCACCCTGGTCACCGTCTCCTCA	QQLEQSGGGLVQPEGSLTLTCTVSGFSWKYDYMCWVRQAPGKGLEWIVCIYGDSGSTWYASWVNGRFTISKTSSTTVTLQMASLTVADTATYFCARADTGAGGYPFNLWGPGTLVTVSS	GCCCTTGTGATGACCCAGACTCCAGCCTCCGTGTCTGAACCTGTGGGAGGCACAGTCATCATCAATTGCCAGGCCAGTCAGAGTATTGGTAGTAATTTAGCCTGGTATCAGCAGAAACCAGGGCAGCGTCCCAAGCTCCTGATGTATGCTGTTTCCAATCTGGCATCTGGGGTCCCATCGCGGTTCAGTGGCAGTGGATCTGGGACAGAGTTCACTCTCACCATCAGCGACCTGGAGTGGGCCGATGCTGCCACTTATTACTGTCAGGGCGGTGCGGTTTTTCATGATGTTGGTTTCGGCGGAGGGACCGAGGTGGTGGTCAAACGT	ALVMTQTPASVSEPVGGTVIINCQASQSIGSNLAWYQQKPGQRPKLLMYAVSNLASGVPSRFSGSGSGTEFTLTISDLEWADAATYYCQGGAVFHDVGFGGGTEVVVKR	This paper
M8a-7 IgG	Mouse	CAGGCTTACCTGCAGCAGTCTGGCGCTGAAATGGTTCGACCTGGCGCCTCCGTGAAGATGAGCTGTAAAGCCAGCGGCTACACCTTCAACAACTACAACATGCACTGGGTCAAGCAGACCCCTAGCCAGGGACTCGAGTGGATCGGCGGCTTTTACCCCGGCAATGACGATACCGCCTACAGCCAGAAGTTCAAGGGCAAAGCCACACTGACCGTGGACAAGAGCAGCAGCACCGCCTTTATGCACCTGAGCAGCCTGACCAGCGAGGACAGCGCCGTGTACTTTTGTGCCAGAAGCCTGGGCCGCTACTACGCCATGGATTATTGGGGCCAGGGCACCAGCGTGACCGTTTCT	QAYLQQSGAEMVRPGASVKMSCKASGYTFNNYNMHWVKQTPSQGLEWIGGFYPGNDDTAYSQKFKGKATLTVDKSSSTAFMHLSSLTSEDSAVYFCARSLGRYYAMDYWGQGTSVTVS	GACATCGTGCTGACACAGAGCCCTGCTTCTCTGGCCGTGTCTCTGGGACAGAGAGCCACCATCAGCTGTAGAGCCAGCGAGAGCGTGGACGACTTCGGCATCAGCTACATGAACTGGTTCCAGCAGAAGCCCGGCCAGACACCTAAGCTGCTGATCTACGGCGCCAGCAATCAAGGCAGCGGAGTGCCTGCCAGATTTTCTGGCTCTGGCAGCGGCACCGACTTCAGCCTGAACATTCACCCCATGGAAGAGGACGACCCCGCCATGTACTTTTGCCAGCAGAGCAAAGAGGTGCCCTACACCTTTGGCGGAGGCACCAAGCTGGAAATCAAG	DIVLTQSPASLAVSLGQRATISCRASESVDDFGISYMNWFQQKPGQTPKLLIYGASNQGSGVPARFSGSGSGTDFSLNIHPMEEDDPAMYFCQQSKEVPYTFGGGTKLEIK	Fan, et al., Immunity, 2022

Extended Data Table 2. Cryo-EM data collection, refinement and validation statistics

	M8b-A10 in complex with SARS-2 spike (EMDB 48347) (PDB 9ML4)	M8b-B8 in complex with SARS-2 spike (EMDB 48348) (PDB 9ML5)	M8b-C9 in complex with SARS-2 spike (EMDB 48349) (PDB 9ML6)	M8b-C10 in complex with SARS-2 spike (EMDB 48350) (PDB 9ML7)
Data collection and processing				
Magnification	105,000x	45,000x	105,000x	105,000x
Voltage (kV)	300	200	300	300
Electron exposure (e–/Å^2)	60	60	60	60
Defocus range (μm)	-1 to -3	-1 to -3	-1 to -3	-1 to -3
Pixel size (Å)	0.832	0.869	0.832	0.832
Symmetry imposed	C1	C1	C1	C1
Initial particle images (no.)	950,884	576,218	1,159,077	1,663,789
Final particle images (no.)	134,713	148,375	132,671	165,304
Map resolution (Å)	3.3	3.4	3.5	3.2
FSC threshold	0.143	0.143	0.143	0.143
Refinement				
Initial model used (PDB code)	7UZD, 7SC1	7UZD, 7SC1	7UZD, 7SC1	7UZD, 7SC1
Model composition				
Non-hydrogen atoms	29,480	27,822	29,751	25,846
Protein residues	3,717	3,491	3,750	3,259
Ligands	58	49	45	35
B factors (Å^2)				
Protein	167.3	125.0	90.0	124.5
Ligand	145.1	120.0	97.2	128.3
R.m.s. deviations				
Bond lengths (Å)	0.003	0.003	0.003	0.004
Bond angles (°)	0.603	0.575	0.610	0.630
Validation				
MolProbity score	1.7	1.8	1.9	2.1
Clashscore	8.3	7.1	9.7	10.4
Poor rotamers (%)	1.2	1.4	1.7	2.5
Ramachandran plot				
Favored (%)	96.7	96.2	96.9	96.3
Allowed (%)	3.3	3.8	3.1	3.7
Disallowed (%)	0	0	0	0

Extended Data Table 3. X-ray Data collection and refinement statistics

	M8b-B1 Fab in complex with SARS-2 RBD (PDB 9ML8)	M8b-C9 Fab in complex with SARS-2 RBD (PDB 9ML9)
Data collection		
Space group	C2	C2
Cell dimensions		
a, *b*, *c* (Å)	175.1, 173.4, 129.9	108.2, 127.2, 75.4
α, β, γ (°)	90, 116.6, 90	90, 127.7, 90
Resolution (Å)	2.40 - 39.14 (2.40 - 2.44)	2.59 - 37.99 (2.59 - 2.71)
R_{merge}	0.172 (0.989)	0.082 (0.983)
$I / \sigma I$	7.3 (2.3)	11.7 (1.7)
Completeness (%)	98.5 (99.1)	98.5 (94.5)
Redundancy	7.2 (7.4)	7.2 (7.1)
Refinement		
Resolution (Å)	2.4	2.6
No. reflections	132,912	24,650
R_{work} / R_{free}	0.223/0.247	0.226/0.257
No. atoms	20,452	4,967
Protein	19,550	4,916
Ligand/ion	147	30
Water	755	23
B-factors (Å^2)	55.2	73.9
Protein	55.4	73.9
Ligand/ion	93.2	91.8
Water	43.6	61.0
R.m.s. deviations		
Bond lengths (Å)	0.002	0.003
Bond angles (°)	0.54	0.55

*Values in parentheses are for highest-resolution shell.

Methods

Mammalian cell lines

HEK293T (pseudovirus production) and HEK293T-hACE2 cells (pseudovirus neutralization assays) were cultured in Dulbecco's modified Eagle's medium (DMEM) supplemented with 10% heat-inactivated fetal bovine serum (FBS, Bio-Techne) and 1% Penicillin/Streptomycin (Gibco) and 1% L-Glutamine (Gibco). HEK-293T cells expressing high levels of hACE2 (kindly provided by Kenneth Matreyek, Case Western Reserve University), used for SHC014 pseudovirus neutralization assays, were cultured in DMEM supplemented with 10% heat-inactivated FBS (Bio-Techne), 1% Penicillin/Streptomycin (Gibco), 1% L-Glutamine (Gibco), 0.75 μg/mL puromycin dihydrochloride (Research Products International) and 2 μg/mL doxycycline hydrochloride (Thermo Fisher Scientific). HEK293T/ACE2cl.22 cells[41] (*in vitro* selection experiments) were cultured in DMEM supplemented with 10% FBS and 10 μg/mL gentamicin. Cell lines were cultured at 37 °C and 5% CO_2.

Expi293F cells for protein expression were maintained in Expi293 expression medium (Thermo Fisher Scientific). Transfections were performed using the Expi293 Expression System Kit and maintained under shaking at 130 rpm at 37 °C and 8% CO_2.

RBD expression and production of RBD-NPs

SpyTag003[39]-tagged RBDs for conjugation and Avi-tagged RBDs for Beacon assays and ELISAs were expressed by transient transfection in Expi293F cells and purified as previously described[32,34]. Briefly, mammalian expression vectors encoding the RBDs of SARS-2 Beta (GenBank QUT64557.1), RaTG13-CoV (GenBank QHR63300), SHC014-CoV (GenBank KC881005), Rs4081-CoV (GenBank KY417143), pangolin17-CoV (GenBank QIA48632), RmYN02-CoV (GSAID EPI_ISL_412977), Rf1-CoV (GenBank DQ412042), W1V1-CoV (GenBank KF367457), SARS-2 Wuhan-Hu-1 (GenBank MN985325.1), SARS-2 Omicron BA.1 (GenBank UFO69278.1), SARS-2 Omicron BA.4/BA.5 (GenBank UPP14409.1), SARS-2 Omicron BA.5-S8[74], SARS-2 Omicron XBB.1(EPI_ISL_15031899), SARS-2 Omicron XBB.1.5 (GenBank UZG29433.1), SARS-2 Omicron JN.1 (GenBank OR816965.1), SARS-2 Omicron KP.3 (EPI_SET_240529sa), RsSTT200-CoV (EPI_ISL_852605), SARS-1 (GenBank AAP13441.1), Yun11-CoV (GenBank JX993988), BtkY72-CoV (GenBank KY352407), Khosta-2-CoV (QVN46569.1), or BM-4831-CoV (GenBank NC014470) with the appropriate tag were used for transfection as described[32,34,45]. Genes for RBDs used for Beacon assays were co-expressed with a plasmid encoding an ER-directed BirA enzyme for *in vivo* biotinylation[75] (kind gift of Michael Anaya, Caltech) using a 1:1 RBD to BirA plasmid ratio for transfections. Biotinylation was confirmed using a gel shift assay with streptavidin. RBDs were purified from transiently-transfected Expi293F supernatants by Ni-NTA and size-exclusion chromatography (SEC) and stored at 4˚C or -80˚C after flash freezing in liquid nitrogen[43].

A soluble SARS-2 Wuhan-Hu-1 spike trimer with 6P stabilizing mutations[43] was expressed and purified[22] for structural studies. Human IgG mAbs and human ACE-2 fused to human IgG Fc (hACE2-Fc)[27] were expressed and purified as described[22,27]. SpyCatcher003-mi3 NPs[38] were produced in *B. subtilis* (Ingenza, LTD) and purified as described[31].

RBD-NPs were generated by incubating SpyCatcher003-mi3 with a 2-fold molar excess (RBD to mi3 subunit) of SpyTagged RBD (either a single RBD for homotypic RBD-NPs or an equimolar mixture of eight RBDs for mosaic-8b RBD-NPs) overnight at room temperature in Tris-buffered saline (TBS). Conjugated RBD-NPs were separated from free RBDs by SEC as described[32]. Concentrations of conjugated RBD-NPs are reported based on RBD content determined using a Bio-Rad Protein Assay.

mAbs for characterization assays

Rabbit mAbs that bind to SpyCatcher (anti-SC003 E1) and mi3 (anti-mi3 A3) were identified from memory B cells from rabbits immunized with mosaic-8b or homotypic RBD-NPs, respectively. Activated PBMCs were loaded on a Beacon chip and assayed for binding to SpyCatcher and mi3. Candidate IgG-secreting B cells were exported and VH and VL gene segments were cloned into expression vectors encoding human constant domains.

Human mAbs that bind to Pang17, SHC014, Rs4081, Rf1, or RmYN02 RBD but not any of the other seven RBDs on mosaic-8b RBD-NPs (anti-Pang17, anti-SHC014, anti-Rs4081, Anti-Rf1 422, Anti-Rf1 425, Anti-Rf1 428, anti-RmYN02) were identified via contract by Biorad using their HuCAL technology with a positive selection and multiple negative selection strategy (Biorad). gBlocks corresponding to V_H and V_L sequences provided by Biorad were cloned into expression vectors encoding human constant domains.

A rabbit mAb (anti-RaTG13 F1) that binds to RaTG13 RBD and not the other seven RBDs on the mosaic-8b RBD-NPs was identified from a rabbit immunized with mosaic-8b RBD-NPs. Activated PBMCs were loaded on a Beacon chip and assayed for binding to the eight RBDs of mosaic-8b and the NP components (mi3 and SpyCatcher). Candidate IgG-secreting B cells were exported and VH and VL gene segments were cloned into expression vectors encoding human constant domains. Candidate mAbs were expressed and screened by ELISA for RaTG13 binding and minimal binding to other antigens.

β38 IgG (binding to SARS-2 Beta RBD) and M8a-7 IgG (binding to WIV1 RBD) were described previously[33,76].

To confirm the appropriate specificity, anti-scaffold and anti-RBD mAbs were expressed and purified by MabSelect SURE affinity chromatography as described in the Ab cloning, protein expression, and purification section below. Purified mAbs were tested for binding to all eight RBDs (anti-RBD mAbs), or for binding to scaffold components (anti-SC003 and anti-mi3 mAbs) in ELISAs as described in the Binding and Competition ELISAs section below. Briefly, 2.5-5 μg of RBD, soluble SpyCatcher003, SC003-mi3, RBD-NPs, or mi3 was coated on MaxiSorp™ 384-well plates (Millipore Sigma) overnight. Excess RBD was removed by aspiration and plates were blocked with 3% bovine serum albumin (BSA). A dilution series of mAb was incubated for 3 hours, followed by incubation with an HRP-conjugated goat anti-human IgG (SouthernBiotech) secondary and detection by luminescence using SuperSignal ELISA Femto Maximum Sensitivity Substrate (Thermo Fisher Scientific). Experiments were conducted in duplicate (anti-RBD mAbs) or quadruplicate (anti-scaffold mAbs) with replicates averaged and standard deviations reported as error bars.

Anti-SC003 E1 and anti-mi3 A3 Fabs were generated from IgGs by incubating activated papain (Sigma-Aldrich) with 1-5 mg of IgG at a 1:100 ratio at 37 ºC for one hour. Fabs were separated from uncleaved IgG and papain by MabSelect SURE column and purified by SEC (Superdex 200 10/300; Cytiva).

A sandwich ELISA was used to characterize the NPs. Briefly, 2.5-5 µg of Fab was adsorbed to MaxiSorp™ 384-well plates (Millipore Sigma) overnight. Excess Fab was removed by aspiration and plates were blocked with 3% BSA. Plates were incubated with 0.25 µg/mL of mosaic-8b RBD-NP, homotypic RBD-NP, or SC003-mi3 for 2 hours at room temperature, followed by incubation with 1 µg/mL IgG for 2 hours. Bound IgG was detected with an Fc-specific secondary conjugated to HRP (goat anti-human IgG Fc; SouthernBiotech) and luminescence was read after incubation with SuperSignal ELISA Femto Maximum Sensitivity Substrate (Thermo Fisher Scientific). Experiments included four technical replicates, which were averaged for visualization.

Mosaic-8b RBD-NP rabbit immunizations

Immunizations were performed by Labcorp Drug Development using IACUC-approved protocols. All procedures in this study design are in compliance with the U.S. Department of Agriculture's (USDA) Animal Welfare Act (9 CFR Parts 1, 2, and 3); the Guide for the Care and Use of Laboratory Animals (Institute of Laboratory Animal Resources, National Academy Press, Washington, D.C., 2011); and the National Institutes of Health, Office of Laboratory Animal Welfare. Whenever possible, procedures in this study are designed to avoid or minimize discomfort, distress, and pain to animals. Five 7-8 week old New Zealand White female rabbits (Envigo) were immunized intramuscularly with 50 µg of conjugated mosaic-8b RBD-NPs (calculated as the mass of the RBD, assuming 100% efficiency of conjugation to SpyCatcher003-mi3, consistent with previous experimental results[34]) in 50% v/v AddaVax™ adjuvant (Invivogen). One female rabbit was immunized intramuscularly with 50 µg of homotypic SARS-2 RBD-NPs in 50% v/v AddaVax™ adjuvant. Animals received 250 µL per quadricep for a total 500 µL administration. Animals were boosted 4 weeks after the prime with a second dose of the same quantity of antigen in adjuvant. Peripheral blood mononuclear cells (PBMCs) and serum were obtained at day 0, 28, 42, 56, 90, and 119. PMBCs were stored at -80 ˚C until use.

Memory B cell activation

PMBCs from were thawed and MACS-enriched as described by Bruker Cellular Analysis in the rabbit Memory B cell workflow (Berkeley Lights, Incorporated). Briefly, PBMCs were thawed at 37 ˚C and drop-wise added to PBMC Thaw Media, centrifuged at 300 x *g* at 4°C, and then resuspended in MACS buffer supplemented with normal mouse serum (Thermo Fisher Scientific 10410) at 5% v/v for blocking. Memory B cells from PBMCs were enriched using MACS with biotinylated anti-IgG (anti-B cell receptor) Ab for labeling of the memory B cells and anti-biotin microbeads (Miltenyi 130-105-637) and MS columns (Miltenyi 130-042-201) for capture and recovery of the labeled cell population. Enriched memory B cells were activated in Activation Media (Bruker Cellular Analysis) for four before loading on the Beacon. PBMC thawing procedures, input cell density, enrichment conditions, and cell density for activation culture were followed from the Bruker Cellular Analysis workflow.

Bruker Cellular Analysis Beacon assays and cell export

Activated PBMCs were loaded on the Bruker Cellular Analysis Beacon instrument at ~8.0 x 10^6 cells/mL. B cells were penned using opto-electero positioning (OEP) into individual nanopens on a 20k or an 11k OptoSelect Beacon microfluidic chip. Assays were conducted by providing a concentrated mixture of 5% goat anti-rabbit IgG (Fc) Coated Polystyrene Particles (Spherotech RPFc-60-5), 1:500 dilution of Alexa Fluor 488 goat anti-rabbit IgG (Jackson 111-546-144) and soluble biotinyated antigens coupled to streptavidin (SA)-fluorophore conjugates. Assay antigens were labeled with biotin via co-expression with BirA and purified and stored in aliquots as described above. Antigens were prepared for Beacon assays by labeling in 10 µg quantities with a 1:0.8 molar ratio of streptavidin-fluorphore conjugates. Conjugates were Streptavidin-Alexa 555 (PE, Thermo Fisher Scientific S32355), Streptavidin-Alexa 680 (Cy5, Thermo Fisher Scientific S32358), and Streptavidin Alexa 594 (TR, Thermo Fisher Scientific S32356) The labeling mixture was incubated at 4 ˚C overnight or until ready for use. The labeled stock was diluted to 20 µg/mL and then used in the assay bead mixture by supplementation to a final individual antigen concentration of 0.5 mg/mL.

Assay images were obtained every 7 minutes for 60 minutes. Multiple assays were run sequentially between 30-minute culture intervals using automated assay bead import. Nanopens were scored as positive or negative for IgG secretion and antigen capture using Bruker Cellular Analysis software for initial scoring and verification by manual inspection for each channel. Scored image sets were intersected to find cells of interest with binding observed for multiple antigens. Cells of interest were exported into 96-well plates containing RIPA (Thermo Fisher Scientific 89901) lysis buffer supplemented with RNAse inhibitor (New England Biolabs (NEB) M0134L) at a final concentration of 2U/µL and 5 mM DTT. This lysis solution was overlaid with mineral oil. Export plates were stored at -70 °C prior to cloning.

Ab cloning, protein expression, and purification

To recover Ig gene sequences of interest, RNA was purified from the single cell exports using RNAClean XP beads (Beckman Coulter A63987) and reverse transcribed into a cDNA library using reagents and guidelines provided by Bruker Cellular Analysis. Intermediate PCR products spanning V_H and V_L domains obtained from individual B cells were confirmed by agarose gel and sequenced by Plasmidsaurus. Gene blocks containing the coding sequences for rabbit V_H and V_L domains obtained from individual B cells were purchased from Integrated DNA Technologies (IDT). Expression constructs were assembled using Golden Gate Assembly (NEB). The heavy chain for IgG expression was constructed by subcloning the V_H gene into a p3BNC expression vector encoding human IgG1 C_H1, C_H2, and C_H3 domains. The expression plasmid for the light chain was constructed by subcloning the V_L gene into a p3BNC vector that also encoded human kappa C_L.

IgGs were expressed in Expi293F cells by transient transfection and purified from cell supernatants using MabSelect SURE columns (Cytiva). Fabs were expressed as His-tagged truncated IgG heavy chains paired with the appropriate light chain and purified by Ni-NTA chromatography. IgGs and Fabs were further purified by SEC using a HiLoad 16/600 Superdex 200 column (Cytiva). Proteins were concentrated using a 30 kDa cutoff concentrator (EMD Millipore) to 10 to 15 mg/mL, and final concentrated proteins were stored at 4 ˚C.

Binding and Competition ELISAs

ELISAs were performed using a Tecan Evo liquid handling robot. For binding assays, Nunc® MaxiSorp™ 384-well plates (Millipore Sigma) were coated with 2.5-5.0 µg/mL of a purified RBD in 0.1 M $NaHCO_3$ pH 9.8 and stored overnight at 4 ˚C. Antigen was aspirated and plates were blocked with 3% bovine serum albumin (BSA) for an hour at room temperature. Blocking solution was removed and 4-fold serial dilutions of purified IgG or supernatant was added and incubated at room temperature for 3 hours. Plates were then washed with Tris-buffered saline with 0.1% Tween-20 (TBST) and incubated with secondary HRP-conjugated goat anti-human IgG (SouthernBiotech) at a 1:100,000 dilution for one hour at room temperature. Plates were washed with TBST, developed using SuperSignal ELISA Femto Maximum Sensitivity Substrate (Thermo Fisher Scientific), and luminescence was measured with a Tecan Infinite M1000 plate reader. ELISA data were collected in quadruplicates. Where indicated, curves were plotted and integrated to obtain half-maximal effective concentrations (EC_{50}) using Graphpad Prism v9.3.1 assuming a one-site binding model with a Hill coefficient. Data points represent the mean and error bars represent the standard deviation of the technical replicates.

Competition ELISAs were performed using a Tecan Evo liquid handling robot. Nunc® MaxiSorp™ 384-well plates (Millipore Sigma) were adsorbed with 5 µg/mL of Fab corresponding to mAb of known RBD epitope in 0.1 M $NaHCO_3$ pH 9.8 and stored overnight at 4 ˚C. Fab was removed and plates were blocked with 3% BSA in TBST for one hour at room temperature. Blocking solution was removed via aspiration and SARS-2 Wuhan-Hu-1 RBD (5 µg/mL) was added and incubated for 2 hours at room temperature. The RBD was removed via aspiration and 1 µg/mL IgG was added and incubated for 2 hours. The plate was washed with TBST and bound IgG was detected using horseradish peroxidase-conjugated Goat Anti-Human IgG Fc (SouthernBiotech) (1 hour, room temperature) and developed with SuperSignal ELISA Femto Substrate (Thermo Fisher Scientific). Luminescence was measured with a Tecan Infinite M1000 plate reader. Measurements were performed in technical quadruplicates and means are shown in a heat map.

Pseudovirus neutralization assays

SARS-2 Wuhan-Hu-1 D614G, SARS-2 VOCs, SARS-CoV, WIV1, SHC014, BtKY72/SARS-1 chimera (including mutations allowing human ACE2 binding[77]), and Khosta2/SARS-1 chimera pseudoviruses based on HIV lentiviral particles were prepared as described[8,78]. BtKY72/SARS-1 and Khosta2/SARS-1 chimeric spikes were constructed by replacing the RBD of the SARS-1 spike with the BtKY72 or Khosta2 RBD as described[32]. Assays were done using 4-fold dilutions of purified IgGs at a starting concentration of 100 µg/mL by incubating with a pseudovirus at 37 ˚C for an hour. After incubating with $293T_{ACE2}$ target cells for 48 hours at 37 ˚C, cells were lysed with Luciferase Cell Culture Lysis 5x reagent (Promega). Luciferase activity in lysates was measured and relative luminescence units (RLUs) were normalized to values derived from cells infected with pseudovirus in the absence of IgG. Data were collected at each IgG concentration in duplicate and averaged. Half-maximal inhibitory concentrations (IC_{50} values) were determined using nonlinear regression in AntibodyDatabase[79].

DMS

DMS studies used to map epitopes recognized by mAbs were performed in duplicates using SARS-2 Beta RBD libraries (generously provided by Tyler Starr, University of Utah) as described previously[80]. RBD libraries were induced for RBD expression in galactose-containing

synthetic defined medium with casamino acids (6.7g/L Yeast Nitrogen Base, 5.0 g/L Casamino acids, 1.065 g/L MES acid, 2% w/v galactose, and 0.1% w/v dextrose). After inducing for 18 hours, cells were washed 2x and then incubated with monoclonal Abs (dilutions chosen to give sub-saturating binding to RBDs) for 1 hour at RT with gentle agitation after which cells were washed 2x and labeled for 1 hour with secondary Ab: 1:200 Allophycocyanin-AffiniPure Goat Anti-Human IgG/Fcγ Fragment Specific (Jackson ImmunoResearch 109-135-098, RRID:AB_2337690) for human mAbs.

Stained yeast cells were processed on a Sony SH800 cell sorter and were gated to capture RBD mutants that had reduced mAb binding but relatively high RBD expression. For each sample, cells were collected up until around 3-5 x 10^6 RBD^+ cells were processed (which corresponded to around 2 x 10^5- 1 x 10^6 RBD^+ Ab escaped cells). mAb-escaped cells were grown overnight in a synthetic defined medium with casamino acids, 100 U/mL penicillin, and 100 µg/mL streptomycin to expand cells prior to plasmid extraction. DNA extraction and Illumina sequencing were carried out as previously described[81]. Raw sequencing data are available on the NCBI SRA under BioProject PRJNA1067836, BioSample SAMN45169522. Escape fractions were computed using processing steps described previously[71,81] and implemented using a Swift DMS program (processing folder and program available from authors upon request). Escape scores were calculated with a filter to remove variants with deleterious mutations that escape binding due to poor expression, >1 amino acid mutation, or low sequencing counts as described[42,81].

Line plot and logo plot visualizations of escape maps were created using Swift DMS[81], where letter height (for logo plot) indicates the escape score for that amino acid mutation, and height of the stack of letters (for logo plot) or line peak (for line plots) indicate the total site-wise escape metric, calculated as previously described[81]. Letters for each site (for logo plots) were colored according to epitope class. For structural visualizations, an RBD surface (PDB 6M0J) was colored by the site-wise escape metric at each site, with red scaled to be the maximum used to scale the y-axis for mAbs. Residues that exhibited the greatest escape fractions were highlighted with their residue number and colored according to epitope class.

In vitro selection experiments

To identify viral escape substitutions in the presence of mAb, we used a recombinant replication-competent vesicular stomatitis virus (rVSV) encoding the spike proteins of either SARS-2 Wuhan-Hu-1, SARS-2 VOC BA.2, SARS-2 VOC XBB.1.5, or SARS-1 as described[41,58]. Briefly, viral populations containing 10^6 infectious units of either rVSV/SARS-2/GFP_{2E1}, rVSV/SARS-2/$GFP_{BA.2}$, rVSV/SARS-2/$GFP_{XBB.1.5}$, or rVSV/SARS-2/GFP_{SARS-1}[41] were incubated with mAb at a concentration 10x above its IC_{50} value for 1 hour at 37ºC. Each virus/mAb mixture was then added to HEK-293T/ACE2cl.22 cells. In parallel, as a control, the four viral populations were added to the cells in the absence of any mAb. After 24 hours, the medium was replaced with fresh medium containing either a mAb or DMEM only. Following another 24 hours, the virus-containing supernatant was filtered through a 0.22 µm 96-well filter plate. The filtered supernatant (100 µL) was then incubated with the same concentration of rabbit mAb for 1 hour at 37ºC, as described above. Each virus/mAb mixture was used to inoculate HEK-293T/ACE2cl.22 cells for a second passage (p2). Medium was again replenished with fresh mAb-containing medium or DMEM only after 24 hours, and the p2 viral populations were

harvested after 48 hours. RNA was extracted from 100 µL of filtered p2 supernatant and reverse-transcribed using the SuperScript VILO cDNA Synthesis Kit (Thermo Fisher Scientific). Sequences encoding the extracellular domain of spike were amplified using KOD Xtreme Hot Start Polymerase (Sigma-Aldrich, 719753). Resulting PCR products were sequenced using Illumina MiSeq Nano 300 V2 cycle kits (Illumina, MS-103-1001) to identify mAb escape substitutions in the RBD. Specifically, sequencing reads were aligned to the corresponding RBD reference sequence and annotated for the presence of mutations. A variant was defined as occurring at a frequency >3% of reads at that position.

Cryo-EM Sample Preparation

Complexes of SARS-2 Wuhan-Hu-1 spike and Fabs were formed by incubating a purified spike trimer and a Fab at a molar ratio of 1:3.3 at room temperature for 30 minutes at a final spike concentration of ~2 mg/ml. Prior to freezing, fluorinated octylmaltoside solution (Anatrace) was added to the spike-Fab complex to a final concentration of 0.02% (w/v). Immediately after detergent addition, 3 µL of the spike-Fab complex/detergent mixture was applied to QuantiFoil 300 mesh 1.2/1.3 grids (Electron Microscopy Sciences) that had been freshly glow discharged for with 1 min at 20 mA using PELCO easiGLOW (Ted Pella). Grids were blotted with 0 blot force for 3 seconds with the Whatman No.1 filter paper at 100% humidity and room temperature before vitrification in 100% liquid ethane using a Mark IV Vitrobot (Thermo Fisher Scientific).

Cryo-EM data collection and processing

Single-particle cryo-EM datasets for complexes of SARS-2 Wuhan-Hu-1 spike 6P with M8b-A10 Fab, M8b-C9 Fab, and M8b-C10 Fab were collected using SerialEM[82] on a 300 keV Titan Krios (Thermo Fisher Scientific) equipped with a K3 direct electron detector camera (Gatan). Movies were recorded with a total dosage of 60 $e^-/Å^2$ and a defocus range of -1 to -3 µm in 40 frames using a 3x3 beam image shift pattern with 3 exposures per hole in super-resolution mode at a pixel size of 0.416 Å. A single-particle cryo-EM dataset for SARS-2 Wuhan-Hu-1 spike 6P–M8b-B8 Fab complex was collected with SerialEM[82] on a 200 keV Talos Arctica (Thermo Fisher Scientific) equipped with a K3 direct electron detector camera (Gatan). Movies were recorded with a total dosage of 60 $e^-/Å^2$ and a defocus range of -1 to -3 µm in 40 frames using a 3x3 beam image shift pattern with one single exposure per hole at a pixel size of 0.4345 Å. For all single-particle datasets, motion correction was performed with a binning factor of 2 using Patch Motion Correction in cryoSPARC v4.3[83]. Contrast Transfer Function (CTF) parameters were estimated via Patch CTF Estimation, and particles were picked with blob picker using a particle diameter of 100 to 200 Å in cryoSPARC v4.3[83]. Following inspection, particles were extracted and 2D classified in cryoSPARC v4.3[83]. After discarding bad particles, the remaining particles were used for *ab initio* modeling with 4 volumes, and these volumes were further refined with heterogeneous refinement in cryoSPARC v4.3[83]. Homogeneous and non-uniform refinements were carried out for the final reconstruction in cryoSPARC v4.3[83]. As the interactions between Fab and RBD were generally not well resolved when the RBDs adopted "up" conformations[23], we used local refinement to refine RBD-Fab regions as necessary. Masks used for local refinements were generated with UCSF Chimera[84] and local refinements were done in cryoSPARC v4.3[83].

Cryo-EM Structure Modeling and Refinement

An initial model of the M8b-A10 Fab–SARS-2 RBD complex was generated by docking a mouse M8a-34 Fab–SARS-2 RBD (PDB 7UZD) into the locally refined cryo-EM density for M8b-A10 Fab–SARS-2 RBD using UCSF Chimera[84]. The docked model was refined in Phenix[85] using real space refinement and the amino acid sequences for the Ab heavy and light chains were manually corrected in Coot[86]. The M8b-A10 Fab–SARS-2 spike complex structure was generated by docking the refined structure of M8b-A10 Fab–SARS-2 RBD and a single-particle cryo-EM structure of SARS-2 spike trimer (PDB 7SC1) into the cryo-EM density map for the M8b-A10 Fab–SARS-2 spike complex in UCSF Chimera[84]. The Fab-spike model was further refined in Phenix[85] using real space refinement, and outlier residues were rebuilt in Coot[86].The refined model of the M8b-A10 Fab was later used as the starting model for the remaining Fabs (M8b-B1, M8b-B8, M8b-C9 and M8b-C10) in the other Fab-spike trimer cryo-EM structures. Iterative real space refinements and model building were carried out separately in Phenix[85] and in Coot[86]. Single-particle cryo-EM statistics are reported in Extended Data Table 2.

X-ray crystallography data collection, processing, and refinement

Crystallization trials for Fab–SARS-2 RBD complexes were set up using commercially available screens by mixing 0.2 μL of well solution and 0.2 μL of protein using sitting drop vapor diffusion[87] on a TTP LabTech Mosquito instrument at room temperature. Crystals for the M8b-B1–SARS-2 RBD were obtained from several conditions. A final dataset was collected from a crystal grown in a JCSG+ screen (Molecular Dimensions) containing 0.2 M lithium sulfate, 0.1 sodium citrate, and 20% (w/v) PEG 1,000. Crystals for the M8b-C9–SARS-2 RBD complex were also obtained from many conditions, and a final dataset was collected from a crystal grown in a PEGRx (Hampton. Research), containing 2% v/v 1,4-dioxane, 0.1M Tris pH 8.0, and 15% (w/v) PEG 3,350. Crystals were cryoprotected in the crystallization solution mixed with 20% glycerol before flash-cooling in liquid nitrogen.

X-ray diffraction data were collected at 100 K at a wavelength of 0.9795 Å at the Stanford Synchrotron Radiation Lightsource (SSRL) beamline 12-2 using an EIGER 2XE 16M pixel array detector (Dectris) with the Blu-ice interface[88]. X-ray datasets were indexed and integrated with XDS[89] and scaled with Aimless[90]. The M8b-B1 Fab–SARS-2 RBD and M8b-C9 Fab–SARS-2 RBD structures were solved by molecular replacement using Phaser in Phenix[85]. Iterative refinement and model-building cycles were carried out in Phenix[85] and Coot[86]. The final refined M8b-B1–SARS-2 RBD structure included 97.8% of residues in Ramachandran favored regions and 2.2% in an allowed region. The final M8b-C9–SARS-2 RBD structure included 97.5% of residues in Ramachandran favored regions and 2.5% in an allowed region. Crystallographic statistics are reported in Extended Data Table 3.

Structural Motif Searches

To identify Ab/RBD structures with a YY motif in CDRH3 that interacts with RBD residues 378-382, we used the structure motif search service at RCSB[91] with PDB ID 7RKU; residues A51, A52, A53, A54, A55, G104, and G105; RMSD cutoff of 2 Å; and an Atom Pairing setting of All Atoms. A second structure motif search was done for a single CDRH3 tyrosine (corresponding to $Y98_{VH}$ in M8b-C9) and RBD residues 378-379 with PDB ID 7RKU; residues A51, A52, G104, and G105; with exchanges of G105 to all amino acids; RMSD cutoff of 1.5 Å; and an Atom Pairing setting of Backbone Atoms.

Data availability

All data supporting the findings of this study are available within the paper and its Extended Data. Raw sequencing data from DMS experiments have been deposited on NCBI SRA under BioProject PRJNA1067836, BioSample SAMN45169522. Models and density maps for cryo-EM structures are deposited in the PDB (9ML4, 9ML5, 9ML6, and 9ML7) and maps are available on EMDB (48347, 48348, 48349, and 48350). Models and electron density maps for crystal structures are deposited in the PDB (9ML8 and 9ML9).

Code availability

A Swift DMS program for processing and visualizing DMS data is available from authors upon request.

Acknowledgements

We thank Jost Vielmetter and the Caltech Beckman Institute Protein Expression Center for protein production, the Caltech Beckman Institute Beacon Center for Single Cell Biology for conducting Beacon experiments, David Veesler for BtKY72 neutralization advice, Songye Chen and the Caltech Cryo-EM facility for cryo-EM data collection, and Jens Kaiser, staff at Stanford Synchrotron Radiation Lightsource, and the Caltech Molecular Observatory for X-ray data collection support. Cryo-Electron microscopy was performed in the Beckman Institute Resource Center for Transmission Electron Microscopy at Caltech. Use of the Stanford Synchrotron Radiation Lightsource, SLAC National Accelerator Laboratory, is supported by the U.S. Department of Energy, Office of Science, Office of Basic Energy Sciences under Contract No. DE-AC02-76SF00515. The SSRL Structural Molecular Biology Program is supported by the DOE Office of Biological and Environmental Research, and by the National Institutes of Health, National Institute of General Medical Sciences (P30GM133894). The contents of this publication are solely the responsibility of the authors and do not necessarily represent the official views of NIGMS or NIH. These studies were funded by the National Institutes of Health (NIH) P01-AI165075 (T.H., P.D.B., P.J.B.), the Caltech Merkin Institute (P.J.B.), Wellcome Leap (P.J.B.), the Coalition for Epidemic Preparedness Innovations (CEPI) (P.J.B.), and the Boehringer Ingelheim Fonds PhD fellowship (V.A.B.). P.D.B. is a Howard Hughes Medical Institute Investigator. This work was supported, in whole or in part, by the Bill & Melinda Gates Foundation grant INV-034638 (P.J.B.). Under the grant conditions of the Foundation, a Creative Commons Attribution 4.0 Generic License has already been assigned to the Author Accepted Manuscript version that might arise from this submission.

Author contributions

Conceptualization: C.F., J.R.K., K.E.M., P.J.B.; Methodology: K.E.M.; Software: A.P.W.; Formal Analysis: C.F., J.R.K., K.E.M., A.A.C., V.A.B.; Investigation: C.F., J.R.K., K.E.M., A.A.C., A.P.W., V.A.B., A.V.R., H.G., P.N.P.G., S.R., J.A., L.N.S.; Resources: J.R.K., K.E.M., T.H., P.D.B.; Writing – original draft: C.F., J.R.K., K.E.M., A.A.C., A.P.W., V.A.B., P.J.B.; Writing – review and editing: all authors; Visualization: C.F., J.R.K., K.E.M., A.A.C.; Supervision: J.R.K., K.E.M., T.H., P.D.B., P.J.B.; Project Administration: J.R.K., T.H., P.D.B., P.J.B.; Funding: T.H., P.D.B., P.J.B.

Competing interest declaration

P.J.B. and A.A.C. are inventors on a US patent application (17/523,813) filed by the California Institute of Technology that covers mosaic RBD-NPs. P.J.B., C.F., J.R.K., K.E.M., and J.A. are inventors of US patent applications filed by the California Institute of Technology that cover the sequences of the Abs described in this publication. P.J.B. is a scientific advisor for Vaccine Company, Inc. and for ProtaBody, Inc.

Bibliography

1 Cox, M. *et al.* SARS-CoV-2 variant evasion of monoclonal antibodies based on in vitro studies. *Nat Rev Microbiol* **21**, 112-124 (2023). https://doi.org:10.1038/s41579-022-00809-7

2 Ambrose, N. *et al.* Neutralizing Monoclonal Antibody Use and COVID-19 Infection Outcomes. *JAMA Netw Open* **6**, e239694 (2023). https://doi.org:10.1001/jamanetworkopen.2023.9694

3 Fung, T. S. & Liu, D. X. Human Coronavirus: Host-Pathogen Interaction. *Annu Rev Microbiol* **73**, 529-557 (2019). https://doi.org:10.1146/annurev-micro-020518-115759

4 Brouwer, P. J. M. *et al.* Potent neutralizing antibodies from COVID-19 patients define multiple targets of vulnerability. *Science* **369**, 643-650 (2020). https://doi.org:10.1126/science.abc5902

5 Cao, Y. *et al.* Potent neutralizing antibodies against SARS-CoV-2 identified by high-throughput single-cell sequencing of convalescent patients' B cells. *Cell* (2020). https://doi.org:10.1016/j.cell.2020.05.025

6 Kreer, C. *et al.* Longitudinal Isolation of Potent Near-Germline SARS-CoV-2-Neutralizing Antibodies from COVID-19 Patients. *Cell* **182**, 843-854 e812 (2020). https://doi.org:10.1016/j.cell.2020.06.044

7 Liu, L. *et al.* Potent neutralizing antibodies against multiple epitopes on SARS-CoV-2 spike. *Nature* **584**, 450-456 (2020). https://doi.org:10.1038/s41586-020-2571-7

8 Robbiani, D. F. *et al.* Convergent antibody responses to SARS-CoV-2 in convalescent individuals. *Nature* **584**, 437-442 (2020). https://doi.org:10.1038/s41586-020-2456-9

9 Shi, R. *et al.* A human neutralizing antibody targets the receptor-binding site of SARS-CoV-2. *Nature* **584**, 120-124 (2020). https://doi.org:10.1038/s41586-020-2381-y

10 Zost, S. J. *et al.* Rapid isolation and profiling of a diverse panel of human monoclonal antibodies targeting the SARS-CoV-2 spike protein. *Nat Med* **26**, 1422-1427 (2020). https://doi.org:10.1038/s41591-020-0998-x

11 Rogers, T. F. *et al.* Isolation of potent SARS-CoV-2 neutralizing antibodies and protection from disease in a small animal model. *Science* **369**, 956-963 (2020). https://doi.org:10.1126/science.abc7520

12 Seydoux, E. *et al.* Analysis of a SARS-CoV-2-Infected Individual Reveals Development of Potent Neutralizing Antibodies with Limited Somatic Mutation. *Immunity* **53**, 98-105 e105 (2020). https://doi.org:10.1016/j.immuni.2020.06.001

13 Astakhova, E. A., Morozov, A. A., Vavilova, J. D. & Filatov, A. V. Antigenic Cartography of SARS-CoV-2. *Biochemistry (Mosc)* **89**, 862-871 (2024). https://doi.org:10.1134/S0006297924050079

14 Planas, D. *et al.* Sensitivity of infectious SARS-CoV-2 B.1.1.7 and B.1.351 variants to neutralizing antibodies. *Nat Med* **27**, 917-924 (2021). https://doi.org:10.1038/s41591-021-01318-5

15 Washington, N. L. *et al.* Emergence and rapid transmission of SARS-CoV-2 B.1.1.7 in the United States. *Cell* **184**, 2587-2594 e2587 (2021). https://doi.org:10.1016/j.cell.2021.03.052

16 Burki, T. K. Omicron variant and booster COVID-19 vaccines. *The Lancet Respiratory Medicine* (2021). https://doi.org:10.1016/s2213-2600(21)00559-2

17 Liu, L. *et al.* Striking Antibody Evasion Manifested by the Omicron Variant of SARS-CoV-2. *Nature* (2021). https://doi.org:10.1038/s41586-021-04388-0
18 Yamasoba, D. *et al.* Virological characteristics of the SARS-CoV-2 Omicron BA.2 spike. *Cell* **185**, 2103-2115 e2119 (2022). https://doi.org:10.1016/j.cell.2022.04.035
19 Konings, F. *et al.* SARS-CoV-2 Variants of Interest and Concern naming scheme conducive for global discourse. *Nat Microbiol* **6**, 821-823 (2021). https://doi.org:10.1038/s41564-021-00932-w
20 FDA. *Pemgarda EUA* https://www.fda.gov/media/177068/download (2024).
21 Zost, S. J. *et al.* Potently neutralizing and protective human antibodies against SARS-CoV-2. *Nature* **584**, 443-449 (2020). https://doi.org:10.1038/s41586-020-2548-6
22 Barnes, C. O. *et al.* SARS-CoV-2 neutralizing antibody structures inform therapeutic strategies. *Nature* **588**, 682-687 (2020). https://doi.org:10.1038/s41586-020-2852-1
23 Pinto, D. *et al.* Cross-neutralization of SARS-CoV-2 by a human monoclonal SARS-CoV antibody. *Nature* **583**, 290-295 (2020). https://doi.org:10.1038/s41586-020-2349-y
24 Piccoli, L. *et al.* Mapping neutralizing and immunodominant sites on the SARS-CoV-2 spike receptor-binding domain by structure-guided high-resolution serology. *Cell* (2020). https://doi.org:10.1016/j.cell.2020.09.037
25 Wang, Z. *et al.* mRNA vaccine-elicited antibodies to SARS-CoV-2 and circulating variants. *Nature* **592**, 616-622 (2021). https://doi.org:10.1038/s41586-021-03324-6
26 Liu, H. *et al.* Cross-Neutralization of a SARS-CoV-2 Antibody to a Functionally Conserved Site Is Mediated by Avidity. *Immunity* **53**, 1272-1280.e1275 (2020). https://doi.org:10.1016/j.immuni.2020.10.023
27 Jette, C. A. *et al.* Broad cross-reactivity across sarbecoviruses exhibited by a subset of COVID-19 donor-derived neutralizing antibodies. *Cell reports* **36**, 109760 (2021). https://doi.org:10.1016/j.celrep.2021.109760
28 Burnett, D. L. *et al.* Immunizations with diverse sarbecovirus receptor-binding domains elicit SARS-CoV-2 neutralizing antibodies against a conserved site of vulnerability. *Immunity* **54**, 2908-2921 e2906 (2021). https://doi.org:10.1016/j.immuni.2021.10.019
29 Jensen, J. L. *et al.* Targeting the Spike Receptor Binding Domain Class V Cryptic Epitope by an Antibody with Pan-Sarbecovirus Activity. *J Virol* **97**, e0159622 (2023). https://doi.org:10.1128/jvi.01596-22
30 Cui, L. *et al.* A cryptic site in class 5 epitope of SARS-CoV-2 RBD maintains highly conservation across natural isolates. *iScience* **27**, 110208 (2024). https://doi.org:10.1016/j.isci.2024.110208
31 Cohen, A. A. *et al.* Mosaic sarbecovirus nanoparticles elicit cross-reactive responses in pre-vaccinated animals. *Cell* (2024). https://doi.org:10.1016/j.cell.2024.07.052
32 Cohen, A. A. *et al.* Mosaic RBD nanoparticles protect against challenge by diverse sarbecoviruses in animal models. *Science* **377**, eabq0839 (2022). https://doi.org:10.1126/science.abq0839
33 Fan, C. *et al.* Neutralizing monoclonal antibodies elicited by mosaic RBD nanoparticles bind conserved sarbecovirus epitopes. *Immunity* **55**, 2419-2435 e2410 (2022). https://doi.org:10.1016/j.immuni.2022.10.019
34 Cohen, A. A. *et al.* Mosaic nanoparticles elicit cross-reactive immune responses to zoonotic coronaviruses in mice. *Science* **371**, 735-741 (2021). https://doi.org:10.1126/science.abf6840

35 Starr, T. N. *et al.* Deep Mutational Scanning of SARS-CoV-2 Receptor Binding Domain Reveals Constraints on Folding and ACE2 Binding. *Cell* **182**, 1295-1310.e1220 (2020). https://doi.org:10.1016/j.cell.2020.08.012

36 Muecksch, F. *et al.* Development of potency, breadth and resilience to viral escape mutations in SARS-CoV-2 neutralizing antibodies. *Immunity* (2021). https://doi.org:10.1016/j.immuni.2021.07.008

37 Weisblum, Y. *et al.* Escape from neutralizing antibodies by SARS-CoV-2 spike protein variants. *eLife* **9** (2020). https://doi.org:10.7554/eLife.61312

38 Bruun, T. U. J., Andersson, A. C., Draper, S. J. & Howarth, M. Engineering a Rugged Nanoscaffold To Enhance Plug-and-Display Vaccination. *ACS Nano* **12**, 8855-8866 (2018). https://doi.org:10.1021/acsnano.8b02805

39 Keeble, A. H. *et al.* Approaching infinite affinity through engineering of peptide–protein interaction. *Proceedings of the National Academy of Sciences* **116**, 26523-26533 (2019). https://doi.org:10.1073/pnas.1909653116

40 Yuan, M. *et al.* A highly conserved cryptic epitope in the receptor binding domains of SARS-CoV-2 and SARS-CoV. *Science* **368**, 630-633 (2020). https://doi.org:10.1126/science.abb7269

41 Schmidt, F. *et al.* Measuring SARS-CoV-2 neutralizing antibody activity using pseudotyped and chimeric viruses. *Journal of Experimental Medicine* **217** (2020). https://doi.org:10.1084/jem.20201181

42 Greaney, A. J. *et al.* A SARS-CoV-2 variant elicits an antibody response with a shifted immunodominance hierarchy. *PLoS Pathog* **18**, e1010248 (2022). https://doi.org:10.1371/journal.ppat.1010248

43 Hsieh, C. L. *et al.* Structure-based design of prefusion-stabilized SARS-CoV-2 spikes. *Science* **369**, 1501-1505 (2020). https://doi.org:10.1126/science.abd0826

44 Scheid, J. F. *et al.* B cell genomics behind cross-neutralization of SARS-CoV-2 variants and SARS-CoV. *Cell* **184**, 3205-3221 e3224 (2021). https://doi.org:10.1016/j.cell.2021.04.032

45 Barnes, C. O. *et al.* Structures of Human Antibodies Bound to SARS-CoV-2 Spike Reveal Common Epitopes and Recurrent Features of Antibodies. *Cell* **182**, 828-842 e816 (2020). https://doi.org:10.1016/j.cell.2020.06.025

46 ter Meulen, J. *et al.* Human Monoclonal Antibody Combination against SARS Coronavirus: Synergy and Coverage of Escape Mutants. *PLoS Medicine* **3**, e237 (2006). https://doi.org:10.1371/journal.pmed.0030237

47 Tortorici, M. A. *et al.* Broad sarbecovirus neutralization by a human monoclonal antibody. *Nature* **597**, 103-108 (2021). https://doi.org:10.1038/s41586-021-03817-4

48 Krissinel, E. & Henrick, K. Inference of macromolecular assemblies from crystalline state. *J Mol Biol* **372**, 774-797 (2007). https://doi.org:10.1016/j.jmb.2007.05.022

49 Wang, Q., Guo, Y., Ho, J. & Ho, D. D. Activity of Research-Grade Pemivibart against Recent SARS-CoV-2 JN.1 Sublineages. *N Engl J Med* **391**, 1863-1864 (2024). https://doi.org:10.1056/NEJMc2410203

50 Olivieri, D., von Haeften, B., Sánchez-Espinel, C. & Gambón-Deza, F. The immunologic V-gene repertoire in mammals. *bioRxjv* (2014). https://doi.org:10.1101/002667

51 Liu, H. *et al.* Human antibodies to SARS-CoV-2 with a recurring YYDRxG motif retain binding and neutralization to variants of concern including Omicron. *Communications Biology* **5** (2022). https://doi.org:10.1038/s42003-022-03700-6

52 Yuan, M. & Wilson, I. A. The D Gene in CDR H3 Determines a Public Class of Human Antibodies to SARS-CoV-2. *Vaccines (Basel)* **12** (2024). https://doi.org:10.3390/vaccines12050467

53 Liu, H. *et al.* Human antibodies to SARS-CoV-2 with a recurring YYDRxG motif retain binding and neutralization to variants of concern including Omicron. *Commun Biol* **5**, 766 (2022). https://doi.org:10.1038/s42003-022-03700-6

54 Song, G. *et al.* Broadly neutralizing antibodies targeting a conserved silent face of spike RBD resist extreme SARS-CoV-2 antigenic drift. *bioRxiv* (2023). https://doi.org:10.1101/2023.04.26.538488

55 Misson Mindrebo, L. *et al.* Fully synthetic platform to rapidly generate tetravalent bispecific nanobody-based immunoglobulins. *Proc Natl Acad Sci U S A* **120**, e2216612120 (2023). https://doi.org:10.1073/pnas.2216612120

56 Brochet, X., Lefranc, M. P. & Giudicelli, V. IMGT/V-QUEST: the highly customized and integrated system for IG and TR standardized V-J and V-D-J sequence analysis. *Nucleic Acids Res* **36**, W503-508 (2008). https://doi.org:gkn316 [pii]

10.1093/nar/gkn316

57 Goike, J. *et al.* SARS-COV-2 Omicron variants conformationally escape a rare quaternary antibody binding mode. *Commun Biol* **6**, 1250 (2023). https://doi.org:10.1038/s42003-023-05649-6

58 Witte, L. *et al.* Epistasis lowers the genetic barrier to SARS-CoV-2 neutralizing antibody escape. *Nat Commun* **14**, 302 (2023). https://doi.org:10.1038/s41467-023-35927-0

59 Wang, Z. *et al.* Enhanced SARS-CoV-2 neutralization by dimeric IgA. *Science translational medicine* **13** (2021). https://doi.org:10.1126/scitranslmed.abf1555

60 Chen, C. *et al.* CoV-Spectrum: analysis of globally shared SARS-CoV-2 data to identify and characterize new variants. *Bioinformatics* **38**, 1735-1737 (2022). https://doi.org:10.1093/bioinformatics/btab856

61 Arevalo, C. P. *et al.* A multivalent nucleoside-modified mRNA vaccine against all known influenza virus subtypes. *Science* **378**, 899-904 (2022). https://doi.org:10.1126/science.abm0271

62 Casadevall, A., Focosi, D., Pirofski, L. A. & Shoham, S. Single monoclonal antibodies should not be used for COVID-19 therapy: a call for antiviral stewardship. *Clin Infect Dis* (2024). https://doi.org:10.1093/cid/ciae408

63 Corti, D., Purcell, L. A., Snell, G. & Veesler, D. Tackling COVID-19 with neutralizing monoclonal antibodies. *Cell* **184**, 3086-3108 (2021). https://doi.org:10.1016/j.cell.2021.05.005

64 Rappazzo, C. G. *et al.* Broad and potent activity against SARS-like viruses by an engineered human monoclonal antibody. *Science* **371**, 823-829 (2021). https://doi.org:10.1126/science.abf4830

65 Wang, E. *et al.* Designed mosaic nanoparticles enhance cross-reactive immune responses in mice. *bioRxiv* (2024). https://doi.org:10.1101/2024.02.28.582544

66 Guo, H. *et al.* Mechanism of a rabbit monoclonal antibody broadly neutralizing SARS-CoV-2 variants. *Commun Biol* **6**, 364 (2023). https://doi.org:10.1038/s42003-023-04759-5

67 Chen, Y. *et al.* Potent RBD-specific neutralizing rabbit monoclonal antibodies recognize emerging SARS-CoV-2 variants elicited by DNA prime-protein boost vaccination.

Emerg Microbes Infect **10**, 1390-1403 (2021). https://doi.org:10.1080/22221751.2021.1942227

68 Richardson, E. *et al.* Characterisation of the immune repertoire of a humanised transgenic mouse through immunophenotyping and high-throughput sequencing. *Elife* **12** (2023). https://doi.org:10.7554/eLife.81629

69 Zhang, Y. F. & Ho, M. Humanization of rabbit monoclonal antibodies via grafting combined Kabat/IMGT/Paratome complementarity-determining regions: Rationale and examples. *MAbs* **9**, 419-429 (2017). https://doi.org:10.1080/19420862.2017.1289302

70 Landau, M. *et al.* ConSurf 2005: the projection of evolutionary conservation scores of residues on protein structures. *Nucleic Acids Res* **33**, W299-302 (2005). https://doi.org:10.1093/nar/gki370

71 Greaney, A. J. *et al.* Complete Mapping of Mutations to the SARS-CoV-2 Spike Receptor-Binding Domain that Escape Antibody Recognition. *Cell Host Microbe* **29**, 44-57 e49 (2021). https://doi.org:10.1016/j.chom.2020.11.007

72 Kabat, E. A., Wu, T. T., Perry, H. M., Gottesman, K. S. & Foeller, C. Sequences of proteins of immunolgical interest. *Department of Health and Human Services, Washington, D.C.* (1991).

73 Battle, G. PDBePISA : Identifying and interpreting the likely biological assemblies of a protein structure. (2016).

74 Cao, Y. *et al.* Imprinted SARS-CoV-2 humoral immunity induces convergent Omicron RBD evolution. *Nature* **614**, 521-529 (2023). https://doi.org:10.1038/s41586-022-05644-7

75 Tykvart, J. *et al.* Efficient and versatile one-step affinity purification of in vivo biotinylated proteins: expression, characterization and structure analysis of recombinant human glutamate carboxypeptidase II. *Protein Expr Purif* **82**, 106-115 (2012). https://doi.org:10.1016/j.pep.2011.11.016

76 Liu, C. *et al.* The antibody response to SARS-CoV-2 Beta underscores the antigenic distance to other variants. *Cell Host Microbe* **30**, 53-68 e12 (2022). https://doi.org:10.1016/j.chom.2021.11.013

77 Starr, T. N. *et al.* ACE2 binding is an ancestral and evolvable trait of sarbecoviruses. *Nature* (2022). https://doi.org:10.1038/s41586-022-04464-z

78 Crawford, K. H. D. *et al.* Protocol and Reagents for Pseudotyping Lentiviral Particles with SARS-CoV-2 Spike Protein for Neutralization Assays. *Viruses* **12** (2020). https://doi.org:10.3390/v12050513

79 West, A. P., Jr. *et al.* Computational analysis of anti-HIV-1 antibody neutralization panel data to identify potential functional epitope residues. *Proc Natl Acad Sci U S A* **110**, 10598-10603 (2013). https://doi.org:10.1073/pnas.1309215110

80 Starr, T. N. *et al.* Shifting mutational constraints in the SARS-CoV-2 receptor-binding domain during viral evolution. *Science* **377**, 420-424 (2022). https://doi.org:10.1126/science.abo7896

81 Hills, R. A. *et al.* Proactive vaccination using multiviral Quartet Nanocages to elicit broad anti-coronavirus responses. *Nat Nanotechnol* **19**, 1216-1223 (2024). https://doi.org:10.1038/s41565-024-01655-9

82 Mastronarde, D. N. SerialEM: A Program for Automated Tilt Series Acquisition on Tecnai Microscopes Using Prediction of Specimen Position. *Microscopy and Microanalysis* **9**, 1182-1183 (2003). https://doi.org:10.1017/S1431927603445911

83 Punjani, A., Rubinstein, J. L., Fleet, D. J. & Brubaker, M. A. cryoSPARC: algorithms for rapid unsupervised cryo-EM structure determination. *Nat Methods* **14**, 290-296 (2017). https://doi.org:10.1038/nmeth.4169

84 Pettersen, E. F. *et al.* UCSF Chimera--a visualization system for exploratory research and analysis. *J Comput Chem* **25**, 1605-1612 (2004). https://doi.org:10.1002/jcc.20084

85 Liebschner, D. *et al.* Macromolecular structure determination using X-rays, neutrons and electrons: recent developments in Phenix. *Acta Crystallographica Section D Structural Biology* **75**, 861-877 (2019). https://doi.org:10.1107/S2059798319011471

86 Emsley, P., Lohkamp, B., Scott, W. G. & Cowtan, K. Features and development of Coot. *Acta Crystallogr D Biol Crystallogr* **66**, 486-501 (2010). https://doi.org:S0907444910007493 [pii]

10.1107/S0907444910007493

87 Dessau, M. A. & Modis, Y. Protein crystallization for X-ray crystallography. *J Vis Exp* (2011). https://doi.org:10.3791/2285

88 McPhillips, T. M. *et al.* Blu-Ice and the Distributed Control System: software for data acquisition and instrument control at macromolecular crystallography beamlines. *J Synchrotron Radiat* **9**, 401-406 (2002). https://doi.org:10.1107/s0909049502015170

89 Kabsch, W. XDS. *Acta Crystallogr D Biol Crystallogr* **66**, 125-132 (2010). https://doi.org:S0907444909047337 [pii]

10.1107/S0907444909047337

90 Winn, M. D. *et al.* Overview of the CCP4 suite and current developments. *Acta Crystallographica D Biological Crystallography* **67**, 235-242 (2011). https://doi.org:10.1107/S0907444910045749

91 Bittrich, S., Burley, S. K. & Rose, A. S. Real-time structural motif searching in proteins using an inverted index strategy. *PLoS Comput Biol* **16**, e1008502 (2020). https://doi.org:10.1371/journal.pcbi.1008502